学位論文

Exploration of the norm of tree design by the actual measurement of mechanical stresses on tree trunk and branches

樹木にかかる力学ストレスの実測による樹形形成規範の探索

平成 24 年 12 月博士(理学)申請

東京大学大学院理学系研究科

生物科学専攻

南野　亮子

Abstract

Trees are always exposed to mechanical stresses, and therefore, must be strong enough to withstand them. Trees can increase the mechanical safety of their trunks or branches against yielding by increasing the thickness of their trunks or branches. It has been considered that trees maintain the form of their trunks or branches as they keep the mechanical similarity to materialize a mechanically economic structure. Several hypotheses have been established for the self-similarity of trees: geometric similarity, uniform stress similarity, and elastic similarity. The latter two hypotheses include mechanical limitations. The hypothesis of uniform stress similarity states that tree trunks or branches take a form that equalizes the distribution of stress along the outer surface of the trunks or branches. On the other hand, the hypothesis of elastic similarity states that the deflection at the tip of a branch is constant regardless of the length of the branch. Several studies have been conducted on the tapering of a tree trunk or branch by using various tree species. However, few studies have directly assessed the distribution of the mechanical state in a branch, which has often been expressed in relation to the external form, for example, the basal diameter vs. length of the branch. Since branches plastically alter their shapes, to discuss strictly the mechanical similarity, it is necessary to directly measure the stress that occurs at each point of the branches because of loads. I have precisely described the stress distribution in a trunk or branch and proposed a novel view of the morphological strategy by which trees cope with mechanical stresses.

In the first study, I examined the relationship between the morphology of a tree trunk and its mechanical environment. Previous studies have discussed the uniform stress hypothesis against the wind force. Further, the literature includes studies that support and refute the uniform stress hypothesis. However, to the best of my knowledge, evidence by the direct measurements of stresses has not been provided yet, despite the need. In this study, I measured

the strain at the surface of a trunk at varying heights generated by the wind force, for one year, by using an isolated *Larix kaempferi* tree of 21-m height and 58-cm diameter at breast height. During the measurement period, the stress calculated from the strain data was higher in the upper portions of the trunk than in the lower portions, regardless of wind speeds, and the difference increased as the wind speed increased. This tendency continued throughout the measurement period, whereas the details of the stress distribution differed to a certain degree between the periods that the tree had leaves and had no leaves. (In the period after defoliation, the trunk was exposed to wind speeds of up to 28.93 m/s.) The results indicate that the upper portions of the trunk of an isolated *L. kaempferi* tree are more susceptible to wind than are the lower portions. The deflection of the trunk recorded at each position was also larger in the upper portions than in the lower portions. From the comparison of the stress due to the wind force with the modulus of rupture, it was estimated that the base of the trunk could withstand winds of up to 200 m/s, which is much higher than the speed that may be observed around the tree.

In the second study, I evaluated the uniformity of mechanical safety and elastic similarity of horizontal branches of *Fagus crenata* and *Abies homolepis*. Lateral branches are different from trunks in the axis direction and load condition. The stress due to the branch's own weight always acts on lateral branches and should have an important effect on the morphology of branches. I calculated the stress generated along the horizontal branches of *F. crenata* and *A. homolepis* by their own weight by using two different measurement methods. The tensile stress and breaking safety factor (i.e., modulus of rupture divided by actual bending stress) calculated from the moment measurement and destructive test data tended to be constant for most sections of the branches of both species, whereas the small portions ($\phi < 2$ cm) of *F. crenata* branches had a higher safety factor than the other sections. Therefore, the smaller portions of the branches seemed to have mechanically tougher shapes on the basis of the branch's own weight, rather

than the larger potions. The bending safety factor for each point of the branches ranged from 4–10. In the individual branches, the tensile stress was slightly larger at the base of the branches and gently decreased along the branch toward the tip; the safety factor became larger towards the tip for both species. However, another set of stress calculations obtained from strain measurements did not show this tendency. Moreover, the strain measurements showed that the stress generated by self-weight is reduced by the effect of reaction wood, especially in the thicker portions of branches, suggesting that the small safety factor in the thicker portions of the branches was the result of overestimating the stress due to the self-weight. From these results, it was indicated that the stress uniformity is maintained along the branches. The elastic similarity of the branches was evaluated with the strain data at the upper and lower surfaces of branches due to the liberation from the self-weight measured for several species, including *F. crenata* and *A. homolepis*. The deflection at each minute section was determined from the strain data. In all branches, the deflection angle was slightly larger at the base, decreased to some extent, and then increased toward the tip. There was not much difference in the distribution of deflection among the individual branches, and therefore the elastic similarity was not denied. In addition, for one year, I measured the strains at the surface of a branch due to dynamic loads such as wind, snow, and rain, and calculated the maximum tensile stress due to such loads during the year. The maximum tensile stress due to these dynamic loads was lower than the stress due to the branches' self-weight. The safety factor in consideration of all loads was over 3.5 for both species, indicating that the branch had acquired a considerably safe structure.

In the third study, I examined Leonardo da Vinci's rule (i.e., the sum of the cross-sectional area of all tree branches above a branching point at any height is equal to the cross-sectional area of the trunk or the branch immediately below the branching point) by using simulations based on two biomechanical models: the uniform stress model and the elastic similarity model.

Model calculations of the daughter/mother ratio (i.e., the ratio of the total cross-sectional area of the daughter branches to the cross-sectional area of the mother branch at the branching point) showed that both biomechanical models agreed with da Vinci's rule when the branching angles of daughter branches and the weights of lateral daughter branches were small; however, the models deviated from da Vinci's rule as the weights and/or the branching angles of lateral daughter branches increased. The calculated values of the two models were largely similar but differed in some ways. Field measurements of *F. crenata* and *A. homolepis* also fit this trend, wherein models deviated from da Vinci's rule with increasing relative weights of lateral daughter branches. However, this deviation was small for a branching pattern in nature, where empirical measurements were taken under realistic measurement conditions; thus, da Vinci's rule did not critically contradict the biomechanical models in the case of real branching patterns, though the model calculations described the contradiction between da Vinci's rule and the biomechanical models. The field data for *F. crenata* fit the uniform stress model best, indicating that stress uniformity is the key constraint of branch morphology in *F. crenata* rather than elastic similarity or da Vinci's rule. On the other hand, mechanical constraints are not necessarily significant in the morphology of *A. homolepis* branches, depending on the number of daughter branches. Rather, these branches were often in agreement with da Vinci's rule.

These studies revealed that the mechanical limitation is considerably important to both trunks and lateral branches, whereas the details of the limitation may be different between trunks and lateral branches. This difference between trunks and lateral branches may be the result of the difference of the role of trunks and lateral branches. In the reevaluation of Leonardo da Vinci's rule, it was revealed that da Vinci's rule does not necessarily accord with the biomechanical model, and it was indicated that it is necessary to replace such an empirical rule with a physical model.

Contents

Abbreviation list

Symbols	Definition	Page
$\hat{Y}_i$	predicted value of the actual observation	56
$\overline{Y}$	average of the actual observations	56
κ	curvature of deflection of the minute section of the trunk	10
φ	pulling angle of the rope	11
α	exponent	21
δ	deflection at the middle of the branch	29
ε	strain (=$\Delta L/L$)	9
η	:= s/λ	50
λ	whole length of the branch	50
ΔL	change in L	9
δ_M	deformation due to the bending moment	97
ε_{NS}, ε_{EW}	strains in the north-south or east-west direction	10
δ_S	deformation due to the shear stress	97
ε_c	strain of liberation from gravity	32
ε_g	strain of liberation from growth stress	32
ε_{wd}	strain in the wind direction	10
A	cross-sectional area of the beam	97
A_M, A_i	cross-sectional area of the mother or daughter i at the branching point	47
B	measure of mean bias	56
D	diameter at the measurement point	10
D_h	diameter at a given height	7
E	young's modulus (the modulus of elasticity)	12, 29
F	pulling force at the cutoff point	27
G	shear modulus	97
I	second moment of area	50
L	initial material length (or the length of the strain gauges)	9, 31
M	moment (=$W\times a$)	27, 46
M_M, M_i	moment that occurs at the branching point of the mother and daughter branches	47
M_h	bending moment at the height of D_h due to the force of the wind	8
P_b	load applied at the middle of the branch	28
SF	safety factor	29
W	load (that acts on a branch, eg., branch's own weight)	27

W_b, W_s	weights of the portion of the branch proximal or distal to the suspension point	28
W_c	weight of the branch portion distal to the cutoff point	27
W_i	weight of daughter i (i = A, B, C)	47
W_l	weight of the largest daughter branch	54
Y_i	actual observation of the dependent variable	56
a	distance between section mn and the loading point	27
b, s	length between the center of gravity of W_b or W_s and the suspension point	28
d	diameter of the section under consideration	11, 27, 46
d_M	diameter of the mother branch	47
d_i	diameter of the daughter i	48
d_s	stem diameter	21
g	distance between the center of gravity and the base of the section of the branch	49
g_i	distance between the center of gravity of daughter i and the branching point	47
h_m	height of the point that the stress was to be calculated	11
h_p	height of the rope attachment point	11
k	number of estimated parameters used in the estimation	56
k_1, k_2, k_3	constants for $d = k_1 s^{3/2}$, $W = k_2 s^4$, or $g = k_3 s$	49
l	length of the branch	31
l_s	span	28
m_M, m_i	distance between the branching point and the measurement point of the mother or daughter i	47
n	number of daughters ramified from one mother branch	54
n_o	number of observations	56
r	radius of curvature of the branch at its base	49
s	length of the section of the branch from the selected point to the tip	48
s_i	length of each daughter branch	51
s_l	length of the longest daughter branch	51
v	wind speed	12
x	distance between the cutoff point and the suspension point	27
x_s	stem length	21
θ	deflection angle of a section to which strain gauges are attached	31
θ_i	branching angle of daughter i	47
σ	stress (at the surface)	11

σ_b	modulus of rupture	12, 28
σ_{sw}	tensile stress at the surface generated by the branch's own weight	28
σ_{wd}	stress in the wind direction	12

1. General Introduction

Trees are always exposed to mechanical stresses, and must therefore be strong enough to withstand them (McMahon, 1973; Mattheck et al., 1993). The mechanical stresses that affect trees include self-weight, wind, rain, snow, and falling objects. Among them, self-weight and wind are considered to be particularly important. The total amount of load that acts on a branch or trunk because of the mechanical environment increases with the size of the branch or trunk. However, the actual effect of the loads on the branch or the trunk does not always increase with the size of the branch or the trunk and can be canceled out by the increased thickness of the branch or trunk. The actual effect, that is, stress or strain at the surface of a branch is inversely proportional to the cube of the branch diameter, according to material mechanics. For this "actual effect", it has been shown that the plant height or the branch length is much lower than the estimated height or the length that would cause the trunk or branch fail due to its own weight in many plant species—the exception being a few palm species—indicating that many plants take a form with low risk of failure (Niklas, 1994a).

On the other hand, there are some drawbacks to the thickening branches or trunk. To ensure efficient photosynthesis for increased growth of the individual, it is essential to invest resources in growth in height or length and leaf production. Growth increase in diameter becomes a negative factor due to the competition for resources between these investments and diameter growth. In order to maintain safety while ensuring high growth rate, a tree must adopt a mechanically "lean" structure. Researchers who have studied the balance between photosynthetic surface and support structures in trees and herbs in terms of biomechanics have concluded that plants have evolved an optimal mechanical design (McMahon and Kronauer, 1976; King and Loucks, 1978; King, 1986; Givnish, 1985). In these studies of the optimal

mechanical design, two hypotheses have been established that are thought to be both resource economical and mechanically stable: the uniform stress hypothesis and elastic similarity hypothesis. The uniform stress hypothesis states that tree diameter is determined such that the stress induced by gravity or wind is uniform at any position on the tree (Metzger, 1893). The elastic similarity hypothesis states that the deflection of the tip divided by the length of the branch or the trunk results in a constant value (McMahon, 1975).

Many studies have tested the two hypotheses by using various plants. However, most of the studies were performed using the ratio between the basal diameter and whole length or whole mass of the branch or trunk. Tree branches exhibit plasticity in their form, and therefore, measurement of the stresses in many positions on the branches is necessary to adequately discuss the hypotheses. However, there are only few studies that have conducted such measurements (Niklas 1999). These measurements provided the fragmentary evaluation of the biomechanical hypotheses. However, evaluations by the direct measurement are not yet enough, especially for lateral branches. Consideration about the difference between tree trunks and lateral branches is not enough either. Therefore, I thought that it was necessary to increase the direct measurement data about trunks and lateral branches, and to reevaluate the hypotheses using these data. In addition, there is an empirical rule about tree morphology, Leonardo da Vinci's rule. This rule has been believed as a rule of tree architecture. However, there is no physical proof about this rule. If either of the biomechanical hypotheses is true, da Vinci's rule is unnatural. Therefore, I thought that it was necessary to perform proper inspection based on a biomechanical theory and actual survey about the validity of da Vinci's rule.

The aim of this study was to clarify a mechanical characteristic of tree structure by describing the distribution of stresses along a branch. Accordingly, I evaluated the validity of the two biomechanical models. I also discuss the strategy of the trees in terms of morphology.

2. Morphology of trunk related to biomechanics

2.1. Introduction

The morphology of tree trunks has long been studied by sylviculturists, and it has been established that tree morphology can be influenced by its mechanical environment (Metzger, 1893; Jacobs 1954). For vertically standing trees, the force of the wind is a significant hazard to their survival (Putz et al., 1983; Schaetzl et al., 1989; Ennos, 1997). Wind is the main cause of disturbance to trees, and the slenderness (the ratio between the height and the basal diameter) of trees changes with the mechanical environment (e.g., wind) (Lundqvist and Valinger, 1996; Valinger et al., 1994; Valinger and Pettersson, 1996; Meng et al., 2006). When considering the mechanical properties of tree form, the most important factor is bending due to wind, and when large distortion occurs due to wind, buckling due to the weight of the tree, which is triggered by the shift in center of gravity of the tree due to the distortion, must also be taken into account.

The safety factor for a trunk can be calculated based on its weight, and this factor has been used to determine the mechanical stability of tree trunks (Greenhill, 1881; King, 1986; Niklas, 1994ab; Tateno, 1991; Tateno and Bae, 1990). Buckling often occurs in trees growing in dense forests when a strong wind blows; therefore, the degree of safety against buckling is an important consideration. The buckling safety factor is expressed as the critical buckling height divided by the actual height of the trunk (McMahon, 1973; Niklas, 1994ab). The buckling safety factor for 111 plant species with self-supporting stems was found to be around four, and was independent of plant size (Niklas, 1994b), whereas values vary among individuals or between plants growing in different environments (King, 1981; King, 1986). For example, trees growing in an open site were found to have a larger buckling safety factor than trees growing in a dense forest (King, 1981).

Several mechanical models of tree morphology (or trunk taper) have been proposed and tested using measurements of the dimensions of real trees. Metzger (1893) suggested that tree trunks take a form that equalizes the distribution of stress along the outer surface of the stem; this is referred to as the uniform stress hypothesis. He predicted that the diameter of the part of the stem below the crown of a tree trunk should vary as the cube root of the distance from the center of the crown, if the yielding stresses acting on the trunk due to static wind forces are to be equalized. In a study evaluating the uniform stress model for several conifer species, Dean et al. (2002) demonstrated that most plants grown in plantations had a β value (for $D_{\mathrm{h}} \propto M_{\mathrm{h}}{}^{\beta}$,) which supports the uniform stress hypothesis, where D_{h} is the diameter at a given height and M_{h} is the bending moment at that height due to the force of the wind. However, results obtained for *Pseudotsuga menziesii* did not support the uniform stress hypothesis (Dean et al., 2002). In contrast, Niklas and Spatz (2000) reported that maximum stress induced by the wind was not constant along the trunk of a *Prunus serotina* tree growing in an open terrain site.

The details of stress distribution in a tree trunk in response to wind loads are not fully understood. In studies such as those described above, efforts have been made to elucidate the details of stress distribution in an indirect manner: the stress generated in tree trunks by wind loads was estimated based on data for the distribution of the wind speed from the top of the tree to the ground and the moment that the plant may generate due to the wind load. Niklas (2000) estimated the distribution of wind-induced stress along the trunk of a tree for several possible wind distributions using the actual dimensions of an isolated tree, and suggested that differences in the wind profile did not have a marked effect on the distribution of the safety factor in the trunk. For a more precise understanding, the relationship between the wind profile acting on a tree and the resulting stress must be investigated. Moreover, the distribution of the stress generated by the force of the wind (and changes in the position of the center of gravity that are

associated with it) along a trunk or a branch may vary with the wind speed, because the effect of changes in the position of the center of gravity may become greater as the wind speed increases. Therefore, measurements of the actual stress distribution in a tree are necessary.

Currently, there is no method to measure stress directly. However, it is possible to measure strain, which is closely related to stress and can be considered an approximate measurement thereof. Direct measurements of strain in tree trunks in the field have been undertaken in several studies by using strain gauges or mechanical extensometers (Moore et al., 2005; James and Kane, 2008; Hale et al., 2012). The relationship between the morphology of a tree trunk and its mechanical environment is important for understanding the maintenance of plantation stands, and studies involving strain measurements have been conducted on trees growing in forest (Hale et al., 2012). However, as they focused on the possibility of individual trees in a stand falling over, these studies measured strain at only one point on each individual tree. To my knowledge, no studies have conducted direct measurements of the distribution of strain.

In the present study, I measured the distribution of the strain and stress in the surface along the trunk of an isolated *Larix kaempferi* tree due to winds of various strengths and ascertained whether the uniform stress hypothesis could be applied to the form of the isolated tree. I used this tree because it located at an open space where wind was expected to be strong enough to affect the tree morphology and power supply could be secured.

2.2. Materials and methods

Materials

An isolated *Larix kaempferi* tree growing in the Nikko Botanical Garden (Nikko, Tochigi, Japan, 36°45’ N, 139°37’ E) 21 m in height and 58 cm in diameter at breast height (DBH) was used for measurement. The mean annual temperature at this location is 12.1°C, and the mean annual precipitation is 2,400 mm. In Nikko City, the prevailing winds are from the east in the daytime and from the west at night, and tend to be stronger in the daytime than at night (see the website of the Japan Meteorological Agency for historic meteorological data at Okunikko and Imaichi). The habitat of the tree studied has not changed for many years.

Measurement of wind induced strain in an isolated Larix kaempferi *tree*

The strain in the surface of several sections of the trunk due to the force of the wind were measured using strain gauges (FLA-5-11-20LJRA, Tokyo Sokki Kenkyujo) and a multi-recorder (TMR-200, Tokyo Sokki Kenkyujo, Tokyo, Japan) from mid-April 2012 to April 2013. Strain (ε) is the extension or the shrinkage of material and is defined as:

$$\varepsilon = \Delta L/L \qquad (1)$$

where ΔL is the change in the material length caused by an additional force, and L is the initial material length. The measurement points were set on the north, south, east, and west sides of the trunk at various heights (1, 4, 6.5, 9, 12.2, 14.3, and 16.5 m above ground). First, an area of bark 5 cm wide × 5 cm long at each measurement point was removed, and the underlying surface was then exposed to the atmosphere for 1 day to allow it to dry. A portion of each exposed surface was then thinly coated with polyester adhesive (PS, Tokyo Sokki Kenkyujo) and the strain gauge was attached using cyanoacrylate adhesive (CN, Tokyo Sokki Kenkyujo, Fig. 1). The

strain gauges were covered with isobutylene-isoprene rubber sheets for waterproofing and with urethane foam to prevent changes in strain values due to wind cooling. Strains in the north-south and east-west directions were detected as the differences between the strains on the north and south, or east and west, sides of the tree at 20 Hz. The differences between the maximum (excluding noise) and average values of the strain for each hourly dataset were then calculated as the strain due to the force of the wind at each wind speed. From the raw data of the strain due to the force of the wind in both directions, I calculated the strain in the wind direction $\varepsilon_{\mathrm{wd}}$ due to the force of the wind using the following equation:

$$\varepsilon_{wd} = \sqrt{\varepsilon_{NS}^2 + \varepsilon_{EW}^2} \quad (2)$$

where $\varepsilon_{\mathrm{NS}}$ and $\varepsilon_{\mathrm{EW}}$ are the strains in the north-south and east-west directions, respectively (Fig. 2).

From $\varepsilon_{\mathrm{wd}}$, the curvature of deflection of the minute section (5-mm length) of the trunk (κ) was calculated as follows:

$$\kappa = \varepsilon_{wd}/D \quad (3)$$

where D is the diameter at the measurement point. I also calculated the lean of the trunk at each measurement point at the moment that deflection occurred as the integral of the curvature of deflection at each micro-section along the trunk. Here, I assumed that the curvature of deflection of each micro-section along the trunk took a value that was identical to that obtained at the closest measurement point.

I also performed measurements of the speed and direction of the wind at a height of 15 m and 20 m away from the measured tree from April 2012 to April 2013 using wind speed sensors (S-WSA-M003 and S-WDA-M003, Onset Computer Corporation, Massachusetts, USA). The results were compared with the wind data for the Okunikko area (8 km away from the measurement site) published by the Japan Meteorological Agency.

Principle of a strain gauge and the half-bridge 2 active method

A strain gauge is a sensor of strain that is often used in the field of engineering. To measure strain, a strain gauge is attached to the surface of the object to be measured. When the object is deformed, the strain gauge extends or shrinks accordingly, causing the electrical resistance of the gauge to increase when the gauge extends and decrease when the gauge shrinks. The resistance values are converted to strain values using a multi-recorder.

In the present study, I used a half-bridge 2 active method to measure strains along the trunk. This method uses a pair of gauges attached to the opposite sides of the object to be measured. The strain data were obtained as the difference between the strain values on both sides of the object. The effect of air temperature can be excluded using this method.

Measurement of Young's modulus along the trunk

In May 2013, I measured the Young's modulus, which determines the relationship between strain and stress, along the trunk to convert the strain data into stress data. A rope was attached to an upper portion of the trunk (17-m height) and was pulled by a car. During the experiment, the pulling force was recorded using a load cell (TCLZ-10KNA, Tokyo Sokki Kenkyujo) in addition to measuring the strain at the surface at each point on the trunk. Stress at the surface at each height on the trunk was then calculated from the pulling force, pulling angle, distance between the pulling point and the strain-measurement point, and the diameter of the trunk at the strain-measurement point. The relationship between the pulling force F and the stress σ at the surface was expressed as the following equation using the formula of material mechanics (Timoshenko, 1955):

$$\sigma = \frac{32\mathrm{F}\cos\varphi\left(h_p - h_m\right)}{\pi d^3} \tag{4}$$

where φ is the pulling angle of the rope; h_p and h_m are the height of the rope attachment point

and the point that the stress is to be calculated, respectively; and d is the diameter of the section under consideration. I then analyzed the relationship between the stresses and strains generated by the pulling treatment at the surface at each height on the trunk using Kyplot (ver. 2.0 beta 15). According to Hooke's law, the relationship among the stress, strain, and Young's modulus is expressed as the following equation:

$$\sigma = E\varepsilon \quad (5)$$

where σ is the stress, E is the modulus of elasticity (Young's modulus), and ε is the average of strains in the extended surface and the compressed surface (only half of the ε_{wd} value was applied here, because ε_{wd} represents the sum of the value of the extension in the upper surface and the absolute value of the shrinkage in the lower surface). Young's modulus was obtained as the slope of an approximate straight line of the stress and strain, where the line represents equation (5). The approximation was performed by the least-squares method using Kyplot (ver. 2.0 beta 15, Kyenslab Inc., Tokyo, Japan).

Calculation of the stress and maximum force of the wind that can be withstood by the trunk

From the measured strains of the trunk and the Young's moduli, I calculated the stresses in the trunk caused by wind. The stress in the wind direction σ_{wd} was calculated using equation (5).

The critical wind speed for the trunk was calculated by multiplying the wind speed by the ratio of σ_{wd} to published data on the modulus of rupture σ_b for green logs of *Larix kaempferi* (Yamamoto et al., 1992; Koizumi and Ueda, 1987; Yoneda, 1987; Yoshino et al., 2010). The average modulus of rupture was 49.7 ± 5.1 MPa (mean ± SD), and this value was used to calculate the critical wind speed, as follows:

$$critical\ wind\ speed = v \times \sigma_b/\sigma_{wd} \quad (6)$$

Here, v is the wind speed at the time when σ_{wd} was observed.

2.3. Results

Wind characteristics of the measurement site

The maximum wind speed recorded during the measurement period was 28.93 m/s. The maximum wind speed when the branches had leaves was 11.8 m/s; much stronger winds were observed from late fall to winter, when the branches had no leaves. On average, the wind speed was ~2–3 m/s lower at the measurement site than at the Okunikko site used by the Japan Meteorological Agency. This difference between the two sites increased with the increase in wind speed in a manner such that the wind speed data at the two sites fitted the equation y = 0.70 x - 2.83 (from May to October, with leaves, R^2 = 0.60) and y = 0.31 x + 1.88 (from November to December, after defoliation, R^2 = 0.67), where y is the difference between the wind speed recorded at the measurement site and that at the Okunikko site, and x is the wind speed at the Okunikko site. Throughout the measurement period, when a strong wind (20–35 m/s) was recorded at the Okunikko site, the wind speed at the measurement site was generally 5–15 m/s lower. Using these relationships and the wind data for the Okunikko site, where the annual maximum wind speed was 55.4 m/s (on 25 September 1966), the annual maximum wind speed at the measurement site was predicted to be 30–40 m/s (~36.5 m/s calculated using the above equation), which is slightly higher than the maximum value obtained during the measurement period at the measurement site.

Measurement of Young's moduli along the trunk

The average of the Young's moduli along the trunk was 7.923 GPa. The value of Young's modulus varied along the trunk and was larger in the upper portions (Fig. 3, R between Young's modulus and the height was 0.65).

Measurement of wind-induced stresses along the trunk of an isolated Larix kaempferi tree

The measurement data obtained when the branches had leaves showed that the strain and stress generated at the surface by the force of the wind increased toward the top of the tree when the wind speed was less than 28.93 m/s, which was the highest speed recorded during the measurement period (Fig. 4). This tendency became extreme, and the difference between the strains recorded in the higher and lower portions of the trunk increased, as the wind speed increased during the period that the trunk supported leafy branches. This tendency also held for the strains experienced during the period that the tree had no leaves, whereas the stress distribution was slightly different. The stresses in the upper portions of the tree generated by a wind speed of 15.23 m/s during the leafless period were slightly larger than those when the wind speed was 11.8 m/s, whereas the strains in the lower portions at the same time were larger than those when the wind speed was 11.8 m/s. This suggests that the effect of defoliation is greater in the upper portions than in the lower portions.

The stress generated by the force of the wind was 17.1 MPa at 16.5 m above the ground and 7.2 MPa at 1 m above the ground when the wind speed was 28.93 m/s, which was the maximum value recorded during the measurement period.

The curvature of deflection κ was higher in sections of the tree trunk in the higher positions than in the lower positions (Fig. 5A). κ increased with wind speed. The effect of wind speed was reduced when the tree had no leaves. The values of κ when the wind speed was 15.23 m/s (in the leafless period) were only marginally different from the values recorded when the wind speed was 11.8 m/s (in the period with leaves). The lean at the highest measurement point (16.5 m above ground) generated by the wind speed of 11.8 m/s (with leaves) or the wind speed of 15.23 m/s (leafless) was 3° (Fig. 5B). The lean of the trunk was less than 10° even during a

strong wind (28.93 m/s) in the upper portion of the trunk.

Critical wind speed along the trunk

The critical wind speed estimated from σ_{wd} for the wind speed of 28.93 m/s was 85 m/s for the upper portions of the trunk and 200 m/s at the base of the trunk (Fig. 6). The critical wind speeds for the tree with or without leaves were similar in the lower portions of the trunk, when comparing the critical wind speed data for the wind speed of 15.23 m/s without leaves with that for the wind speed of 10.66 m/s with leaves. However, in the comparison mentioned above, in the upper portion, the critical wind speed was greater for the tree without leaves than for the tree with leaves. The calculated critical wind speed was lower when the wind speed at the time that σ_{wd} was observed was large, indicating that a strong wind affects the tree more strongly than a gentle wind because of the impact on the tree at the time of wind loading. This might happen because bigger displacement happened with the high wind speed by resonance.

2.4. Discussion

During the year-long measurement period, the strain gauge performed well in detecting dynamic strain due to wind, although noise was often present in the measurement data. To evaluate the accuracy of the data gathered during the measurement period, in May 2013, I attached new strain gauges adjacent to those that were placed in the lowest position on the tree in April 2012. The new and old gauges recorded identical strain variation in response to wind, thus confirming the accuracy of the old gauges. This indicates that strain gauges attached to the surface of a tree trunk in the manner presented here can detect strain accurately for at least 1 year, unless they become disconnected. Disconnection of a wire was observed in only 2 of 14 sets of gauges during the measurement period. Variation in the fiducial values of strain was rare, except for in the north-south direction at the lowest position. This might have been due to differences in the thermal or water (in wood) conditions of the two gauges. Because the new gauges did not display much variation, the cause was unlikely to be due to variation in the water content of the wood at the surface to which each strain gauge was attached. However, deformation was accurately detected in this data set.

The values of Young's modulus recorded in this study did not differ from the published data (Fig. 3). There was variation in Young's modulus along the trunk; the lower portions of the trunk had smaller Young's moduli than the upper portions, indicating that the wood of lower parts of the trunk were more flexible than that of the upper parts. Variation in Young's modulus along the trunk has been reported in several studies. Brüchert and Gardiner (2006) reported that in a Sitka spruce (*Picea sitchensis*) the Young's modulus was lower in the upper portions than in the lower portions of the trunk. This tendency was also reported by Blackburn (1997) and Brüchert et al. (2000). Radial variation in Young's modulus within a tree trunk has been

reported (Niklas, 1997ab). In specimens of different ages obtained from several locations within a cross section of the trunk of *Robinia pseudoacacia* L., Niklas (1997a) found that the Young's modulus of the wood decreased radially from the pith toward the bark. In a specimen obtained from the heartwood near the periphery of the trunk of *Robinia pseudoacacia* L., Niklas (1997b) found that Young's modulus increased with the distance from the top of the tree. According to these studies, the decrease in the local Young's modulus of a tree trunk may vary in relation to the local age or size of portions of the trunk. The variation in Young's modulus observed in this study contradicts these earlier reports. Further measurements are needed to determine whether the variation in Young's modulus observed in this study is a general feature of *Larix kaempferi* trees.

The strain measurements demonstrated that the stress generated by wind loads was greater in the upper positions of the trunk when the wind was not extremely strong (Fig. 4). The distribution of the stress along the trunk differed between the period when a tree had leaves and the period after defoliation. The strain in the upper positions resulting from a 15.23-m/s wind when the tree had no leaves was only marginally different from that resulting from an 11.8-m/s wind when the tree had leaves, unlike the strain in the lower positions, where a marked difference was observed between the two situations. This indicates that leaves have quite a strong effect, such that the effect of a wind speed of 11.8 m/s on the upper part of a trunk with leaves is almost equal to the effect of a wind speed of 15.23 m/s on the upper part of a trunk without leaves. Furthermore, these findings suggest that the presence of leaves has less effect on wind-induced strain in the lower part of a trunk than in the upper part.

It was assumed that wind deflection might generate stress in the lower portions of a trunk due to the weight of the top of the trunk, increasing the total stress generated in the lower portions of the trunk when wind loads resulted in large deflection. Therefore, it was expected

that the difference between the strain in the upper and lower portions would be reduced or reversed as wind speeds increased. However, trunk deflection was not large during the measurement period, even at a wind speed of 29 m/s; therefore, it is unlikely that this tree would be deflected to an extent that its weight would threaten its survival. Hence, the lower part of the trunk may be less susceptible to the force of the wind than the upper part for winds of strengths typical at the measurement site.

The critical wind speeds for all locations along the trunk were higher than the highest wind speed recorded at Nikko. Therefore, the probability of breakage for parts above ground is low at the plant level. The calculated critical wind speed required for trunk breakage suggests that the probability of breakage at locations near the base is very low for the trunk, considering actual wind speeds in Nikko (<60 m/s). Therefore, if breakage of the trunk occurs, the breaking point will likely be in the upper part of the trunk. The tree used in this study was isolated and was growing in an open site with a severe wind environment compared to locations inside a forest; therefore, its resistance to wind may be greater than for trees growing inside a forest (*i.e.*, the form of an isolated tree can be considered more wind-resistant than that of trees growing inside a forest). By the way, the calculated value of critical wind speed was different among different wind speed. This may be the result of resonance. The time before coming back after a tree bent gets larger with the wind speed. When wind blows before a tree restores after it bend by wind, the tree bends more. As a result, stronger stress would occur inside the tree.

I found that the lower parts of the trunk of an isolated *Larix kaempferi* tree were more secure than the upper parts. This is contrary to the uniform stress hypothesis and supports the conclusion that Niklas and Spatz (2000) derived from the calculation of stress in a trunk of *Prunus serotina* Ehrh. due to the force of the wind. It is likely that other factors (e.g., limitation due to water transportation) affect the radial growth of tree trunks in trees as large as that used

in this study, rather than the mechanical optimality of the tree form (Niklas and Spatz, 2004). In a study of hydraulic limitation on tree form, Niklas and Spatz (2004) produced a model using the scale of an actual tree that produced more consistent results than a model that assumed mechanical stability. Modeling of tree growth that includes water transportation might identify the mechanism that determines (or constrains) tree scale. Taneda and Tateno (2004) reported that biomass distribution (partitioning) to the stem is consistent with the minimum value required for mechanical support (and is not consistent with the optimal value for hydraulic function) in angiosperm trees, whereas the biomass distribution of gymnosperm trees is more similar to the hydraulically optimal value than to the minimum value required for mechanical support. Therefore, it is likely that the hydraulic limitation on tree form is the dominant factor limiting the tree morphology of gymnosperms. However, biomass distribution to the stem in gymnosperms is also close to the minimum value required for mechanical support; therefore, whether the morphology of the stem is limited by mechanical or hydraulic elements remains unknown. In addition, the hydraulic limitation hypothesis predicts that tree height is hydraulically limited (Ryan and Yoder, 1997). Ryan et al. (2006) reviewed the studies of this hypothesis and reported that hydraulic limitation appears to operate in many, but not all, trees. These studies suggest the possibility of the existence of a hydraulic limitation on tree morphology (or scaling). Differences in the microenvironment of individual leaves or branches (e.g., leaves in the upper and lower parts of a tree) may cause differences in their productivity or physiology, which suggests that non-mechanical elements limit the thickness of the tree.

Moreover, it is possible that trees adopt such a structure due to its biomechanical merit. The merit of the structure of a trunk in which the lower portion is less susceptible to an external load than the upper portion, as found in this study, may be that the plant can abandon the upper portion in an emergency and protect the lower portion from breakage, or the plant can reduce

the stress in the lower portion generated by an external load by parrying the load acting on the upper portion. As mentioned previously, even the upper portion that is relatively susceptible to mechanical stress has sufficient strength to endure destruction, which supports the second possibility that plants reduce stress by parrying the wind acting on the upper portion. It is necessary to investigate the effect of this reduction in stress on the minimum biomass distribution to the trunk required to attain biomechanical safety. At least for the trunk of an isolated tree, if there is a strong limitation related to mechanical safety, the key to obtaining the mechanically optimal form may not be the uniformity of stress but may involve another pattern of stress distribution. Alternatively, another mechanical factor may limit the trunk taper.

It is also possible that none of the factors which are considered to limit tree morphology described above is always singly dominant within various tree growth environments. The most important factor for the survival of a tree may change according to the environment in which it grows. It is therefore possible that the limiting factor of tree morphology may also change according to the local environment. Further studies are required to determine the relationship between the environment and tree morphology, from mechanical, hydraulic, and physiological viewpoints, to elucidate the mechanisms of tree design.

3. Mechanical properties of lateral horizontal branches according to their form

3.1. Introduction

For the morphology of lateral branches, an allometric model was derived by McMahon and Kronauer (1976) from two biomechanical hypotheses, the uniform stress hypothesis and the elastic similarity hypothesis. The allometric model of the uniform stress hypothesis is $x_s \propto d_s^{\alpha}$, where $\alpha = ⅔$, and the model of the elastic similarity hypothesis is $x_s \propto d_s^{\alpha}$, where $\alpha = ½$, where x_s is the stem length and d_s is the stem diameter. McMahon and Kronauer (1976) found that the actual allometric relationship was identical to the elastic similarity predictions (assuming a virtual tip in which the branch taper becomes zero distal to the real tip). Bertram (1989) also considered the allometric relationship between the length and diameter of tree stems using the same models, but arrived at a different conclusion. He found that the distal stem elements of a tree can be disproportionately slender, such that x_s scales with respect to the d_s in a manner that exceeds that predicted by the allometry of geometric self-similarity (*i.e.*, $x_s \propto d_s^{\alpha}$, where $\alpha = 1$), whereas the older elements of a tree trunk tend to scale in a manner that approximates elastic self-similarity predictions. Other studies have suggested that the allometry of tree height and trunk taper progressively changes over the course of growth and development (Niklas, 1995; Dahle and Grabosky, 2010; Watt and Kirschbaum, 2011). Niklas (1995) suggested that trees comply with geometric self-similarity in their young portions and subsequently give the appearance of elastic or stress self-similarity as these portions age and become larger. However, which biomechanical model best reflects branches in nature is debatable.

These allometric relationships between the diameter and length can be obtained only on the

assumption that branches maintain complete similarity. Indeed, branch shape is strongly influenced by the light environment and changes plastically. Each part of the branch may not grow larger uniformly, and which part of a branch grows larger depends on its environment. If an imbalance exists in the light environment, the part of a branch that is exposed to stronger light would grow larger than other parts, creating a nonsimilar shape.

In studies of this hypothesis, insufficient work has been done pertaining to the difference between trunks and lateral branches, and some differences may exist in the environment and structure between trunks and lateral (especially, horizontal) branches. Xylem in stems and branches is constructed of nonuniform material (Gartner, 1995), and differences in the microfibril angle in the xylem cell wall also occur at different positions in a branch (Färber et al., 2001), which influences the mechanical properties of wood (Reiterer et al., 1999; Burgert and Fratzl, 2009). Moreover, lateral branches are always subjected to a bending stress due to their own weight, and the mechanical properties of wood are influenced by the plant's reaction against its own weight. Reaction wood is an important element of this reaction, and it has a special internal structure and possesses mechanical properties that are different from normal wood, which is believed to contribute to the correction of the form of a trunk or branch by generating internal stress against the self-weight or an external load (Wilson and Archer, 1997). Bonser and Ennos (1998) questioned the influence that the existing stress has on the safety factor inside of the tree trunk. Few studies, however, have confirmed the uniform stress hypothesis for lateral branches with direct measurements of the real mechanical state induced by loading and the mechanical properties of branches.

For these reasons, I considered that direct measurement of the mechanical properties of branches was necessary to determine the relationship between the morphology and the mechanical state of branches. In this report, I will discuss the stress state of each part of a

branch, which cannot be explained only by the allometry of branches.

To determine mechanical safety, the safety factor, which represents the ratio between the stress needed for the rupture of an object and the actual stress occurring in the object, is useful (Niklas, 1999). For lateral branches, breakage caused by bending is important to consider. Therefore, the safety factor for lateral branches is defined as the ratio of the modulus of rupture to the actual stress generated in a branch by a bending force (breaking safety factor). Measurement of the breaking safety factor has been performed in some recent studies (van Gelder et al., 2006; Anten and Schieving, 2010). Van Gelder et al. (2006) reported the breaking safety factor of lateral branches for saplings of 30 Bolivian rain forest tree species based on the ratio between the actual diameter and the diameter of the limit of rupture due to the weight of the branch. The safety factor is often calculated based on visible characteristics, such as diameter/diameter, as well as stress/stress. The two are the same safety factors, but the values are different. In their study, the breaking safety factor of lateral branches (actual diameter/diameter limit of rupture due to the weight of the branch) ranged from 1.5 to 2.5, which is equivalent to 2.7–14.3 if the safety factor is based on the stress/stress value (van Gelder et al., 2006). However, they did not consider the safety factors of multiple points along a branch. Niklas and Spatz (2000) calculated the safety factors against wind loadings for stems and branches of *Prunus serotina* growing in an open site, and concluded that the safety factor was not uniform throughout the mechanical infrastructure of the trees, although the angles of branches were not noted and the results of the safety factors of stems and branches were not separated. Evans et al. (2008) reported the variation in moment along branches of several shrub species and concluded that the bending stress along the branches was relatively constant, but they did not consider variation in the safety factors of branches.

In previous studies, data from part of a branch have been used as an index of safety for the

whole branch despite evidence supporting the elastic similarity model. As noted previously, the elastic similarity hypothesis and the uniform stress hypothesis are incompatible if a branch is assumed to be a cantilever beam that maintains a completely similar figure, which suggests that the safety factor measured in a part of a branch does not necessarily reflect the safety of the whole branch. Conversely, the elastic similarity hypothesis is likely to be compatible with the uniform stress hypothesis, depending on the style of branching.

Stress due to the dynamic load such as that created by wind, rain, and snow is also important for the mechanical safety of tree branches. Such dynamic loads threaten the mechanical safety of branches by adding additional stress to the interior of branches. An estimation of this stress has been performed by calculating the moment from the wind velocity and placing a projection chart onto the branch or the trunk. Direct measurements have been rarely been performed. However, one study considered the rain load that acts on a horizontal branch using strain gauges (Huang et al. 2005). By using a similar method, the effect of dynamic loads that act on a horizontal branch during a year can be detected.

In this study, I measured the mechanical safety of actual horizontal branches that were considered to be strongly influenced by the constant load of the branch's own weight. More specifically, I measured the stress generated by a branch's own weight and calculated the safety factors for breakage at multiple points along each branch to confirm whether mechanical safety was constant along a branch or among branches (i.e., confirmation of the uniform stress hypothesis). I used two different methods, measurement of the moment and measurement of the strain, to quantify the stress generated by a branch's own weight and investigated whether the stress was constant. In this measurement, I considered the growth stress (see below) inside the branches in addition to their own weight. The strain measurement data were also used to confirm the elastic similarity hypothesis. I also made a measurement of the stress generated by

dynamic loads for horizontal branches of *Fagus crenata* and *Abies homolepis*. I used these species because there were many trees of these species that could be used for the measurements in Nikko Botanical Garden and there is much information about these species.

Finally, I explain about growth stress. During the maturation of wood, deformation occurs in xylem cells. However, due to adhesion to the adjacent cell, deformation is prevented and the stress of deformation is gradually accumulated during secondary growth (Plomion et al., 2001). This stress is called "growth stress." The magnitude of deformation is different between reaction wood and normal wood, and this difference creates a stress gradient inside the branch. Branches and trunks are believed to correct their direction by creating reaction wood. Reaction wood in coniferous species is called compression wood and is produced in the lower section of a leaning trunk where it generates compression stress in the lower section. In broad-leaved species, reaction wood is called tension wood and is produced in the upper section of the trunk. Tension wood is thought to generate a stress gradient by limiting its longitudinal extension during maturation (Burgert and Fratzl, 2009). Measurements of growth stress have been made by tree physiologists using strain gauges (Yamamoto et al., 1989; Yoshida and Okuyama, 2002).

3.2. Materials and methods

Materials

Lower horizontal branches of approximately 30-year-old *Fagus crenata* and *Abies homolepis* trees growing in the Nikko Botanical Garden (Nikko, Tochigi, Japan; E139°37', N36°45', where the mean annual temperature is 12.1ºC and the mean annual precipitation is 2,400 mm), were used for the measurements. Six *F. crenata* and seven *A. homolepis* branches were measured. The average height of the *Fagus* trees was 14.1 ± 2.7 m (mean ± SD) and the average diameter at breast height (DBH) was 23.9 ± 6.6 cm (mean ± SD). The average height of the *Abies* trees used for measurements was 13.8 ± 5.5 m and the average DBH was 31.6 ± 13.1 cm. The habitats of the trees had experienced little environmental change over a period of many years.

Measurements of the morphological characteristics of the branches

I recorded an overview of each branch and the slope at several points along the branch while it was still attached to the trunk. I also measured the diameters of the branches at several points in both the horizontal and vertical planes.

Calculation of stress

When considering the safety of a branch, the tensile stress at the surface of the branch or trunk is important. When a branch is loaded as shown in Fig. 7, its internal mechanical state results in the generation of tensile stress on the upper side and compressive stress on the lower side. Breakage caused by bending limits the safety of branches, and such breakage occurs when the tensile stress at the upper surface (maximum tensile stress in the cross section) reaches a certain limit. The stress uniformity in the uniform stress hypothesis depends on the constancy of the

tensile stress at the surface at any position on the branch, and therefore, measurements of this stress are required. According to material mechanics, the relationship between a load *W* and the tensile stress at a surface is expressed as follows (Timoshenko 1955):

$$\sigma = \frac{32M}{\pi d^3} \tag{7}$$

where *M* is the moment (= *W* × *a*, where *a* is the distance from the load point) and *d* is the diameter at section *mn* in Fig. 7. Although the load is expressed here as intensive load, this equation can be applied to the distributed load, such as the load that acts on a branch (self-weight plus, e.g., wind, rain, and snow). Assuming a distributed load, *M* is calculated as the grand total of the moments generated by the loads acting on each position of the branch.

Measurement of the moment and calculation of the tensile stress at the surface of branches

The moments at several points along each branch were measured to calculate the tensile stress at the surface of the branch. First, a primary branch was cut off at the base and suspended using a rope, as shown in Fig. 8. The point of suspension was set to the left of the center of gravity of the branch, causing it to tilt downward toward the right. A spring balance was attached to the cut end and pulled down until the branch balanced horizontally. The pulling force *F* and the distance between the cutoff point and the suspension point were recorded. Measurement of *F* was repeated, after cutting off a proximal portion between the point where the moment was to be measured and the proximal end of the branch. The length of each portion was determined to ensure a sufficient length to perform a bending test. After these measurements, the weights of the portions of the branch distal or proximal to the suspension point were recorded. From these data, the moments that acted on the cutoff points due to the branch's own weight were calculated using

$$M = \left(F + W_c\right) x \tag{8}$$

where F is the pulling force at the cutoff point, W_c is the weight of the branch portion distal to the cutoff point, and x is the distance between the cutoff point and the suspension point. This equation was derived from the combination of the following equations:

$$bW_b + xF = sW_s \tag{9}$$

$$M = W_s(s + x) + W_b(x - b) \tag{10}$$

$$W_c = W_s + W_b \tag{11}$$

where W_b and W_s are the weights of the portion of the branch proximal or distal to the suspension point, and b and s are the lengths between the center of gravity of W_b or W_s and the suspension point, respectively.

I used the method described above to determine the moment because the method that calculates the moment from the weight and the distance from the center of mass was assumed to produce an error. However, from the measured data, an improvement of the accuracy clearly was not obtained using the method described here. I also calculated the tensile stress at the surface (σ_{sw}) using equation (7) and the data obtained by the above measurements.

Destructive tests

Destructive tests (three-point bending test) were performed on the branches used to measure the moment due to self-weight, and the modulus of rupture σ_b was recorded using a universal testing machine (Tensilon UTM-3-500, Toyo Baldwin Co., Ltd., Tokyo, Japan). σ_b was calculated as

$$\sigma_b = \frac{8P_b l_s}{\pi d^3} \tag{12}$$

where P_b is the load applied at the middle of the branch, l_s is the span, and d is the diameter at the middle of the branch. The span was fixed to 280 mm for thinner (less than about 2.5 cm) branches and 420 mm for thicker branches, and the loading speed was set to 10 mm/min. Green logs with bark cut from the branches used for the measurements described above were set

upside down so as to load from the lower side. Young's modulus, *E*, at each section of the branches was also obtained with this test by using the following equation:

$$E = \frac{4P_b l_s^{\,3}}{3\pi d^4 \delta} \tag{13}$$

where δ is the deflection at the middle of the branch when P_b is smaller than the proportional limit. The Young's modulus data were fitted to a curve by the least-squares method or averaged using KyPlot (version 2.0 beta 15) for the stress calculation based on the strain measurement described in the next section.

In the bending test, the ratio between the height of a square beam and the span should exceed 14 to minimize the effect of shear stress. The height of the beam is here replaced by the diameter of the branch. The span could not be set longer because of the specification of the machine and a slight effect of shear stress that would be included in the measurement data. Therefore, I also performed the calculations to eliminate shear stress from the calculated Young's modulus (Appendix). This is a useful excercise, although the result is less reliable than the real value when the test is performed with an appropriate span/diameter ratio.

Calculation of the safety factor

From these measurements, the breaking safety factor *SF* against each branch's own weight was determined using the following equation:

$$SF = \frac{\sigma_b}{\sigma_{sw}} \tag{14}$$

Measurement of strains in branches

To find the value of σ_{sw} due to the branch's own weight and the influence of the reaction wood (growth stress), I also performed the measurement using another method.

Measurement of strains generated by the liberation of branches from their own weight and growth stress

Using lower horizontal branches of *F. crenata* and *A. homolepis* of a similar size and taken from a similar environment as the branches used for the measurements described above, I investigated the strain on the upper and lower surfaces of branches due to the liberation of the branch from its own weight.

For the measurements, I chose several positions along a branch and debarked an area of appropriate size on the upper and lower surface at each position. Then I attached strain gauges (FLA-5-11-5L, Tokyo Sokki Kenkyujo Co., Ltd.) to each debarked surface in the direction of the longitudinal axis while the branch was still attached to the trunk. At each position, the diameter including the bark both in the horizontal and vertical planes, and diameter without the bark in the vertical plane, were measured with a digital caliper. Strain gauges were connected to a multi-recorder using the half-bridge 2 active method, so that the recorded strain value represented the difference in strain between the upper and lower surfaces, and increased with downward deflection and decreased with upward deflection. The initial strain values (when the branches were still attached to the trunk) were set to zero. Then I cut the branch off at its base and laid it sideways on the ground so that the upper and lower surfaces of the branch faced sideways. After 10 min, I cut the branch into pieces ranging from 30 to 80 cm in length and laid them on the ground again. Changes in the recorded strain values before and after these treatments were recorded as the strain (ε, refer to equation (1)) of each branch due to liberation from its own weight. In this study, I call the above process "liberation from gravity."

To confirm the elastic similarity hypothesis, the deflection of each measurement point along the branches was also calculated from these strain data. Because the elastic similarity

hypothesis states that the deflection at each position of a branch maintain constancy regardless of branch size, I focused on whether the deflection of microsections of the branches at each relative position was constant. The deflection angle, θ, of a section to which strain gauges are attached was determined as

$$\theta = \frac{2\varepsilon L}{d} \tag{15}$$

where L is the length of the strain gauges. The angle θ includes the influence of the length. Therefore, the influence of the length must be eliminated to compare θ among branches with different lengths. The calculation of the deflection angle of the whole branch (i.e., the change in the angle of the tip before and after the loading), assuming that the displacement in this microsection occurred in the same way at all positions of the branch, is effective for comparison of the magnitude of deflection among branches, eliminating the influence of length of the strain gauges relative to the branch length. Therefore, I generated an expression that expresses the relative magnitude of displacement by dividing equation (15) by L/l, where l is the length of the branch. Here, I call the expression the "displacement contribution degree." The displacement contribution degree can be written as

$$\text{displacement contribution degree} = \frac{2\varepsilon l}{d} \tag{16}$$

Then I compared the displacement contribution degree along each branch or among the branches.

Growth stress inside a branch might be operating against its own weight. Therefore, I performed an experiment that released the growth stress from branches to determine the effect of the growth stress on the stress in branches. First, I made a cut at a depth of 1 cm at a position 1 cm from the top and bottom of the strain gauges (Fig. 9). Second, I cut off the branch at the position where the cut was made. Then I notched the wood about 1 mm away from the top and

bottom of the strain gauges using a cutter. Through this series of treatments, I released the growth stress that was stored in the branches. The changes in the strain value during the treatment were recorded for both the upper and lower surface. The strain obtained from this treatment is called “residual strain.”

The stress that a branch experiences in its natural state may be the stress that deducted the element of residual stress from the stress generated by the liberation of the branch from its own weight; i.e., the strain that a branch experiences in its natural state is expressed as $\varepsilon_c + \varepsilon_g$, where ε_c is the strain of liberation from gravity and ε_g is the strain of liberation from growth stress. I defined this strain value as the actual strain experienced in nature.

All of the strains determined from a series of measurements were converted into tensile stress at the surface using equation (5) and the approximate expression of Young’s modulus obtained from the destructive test described above. I also applied the Young’s modulus measured for branches of *F. crenata* and *A. homolepis* using strain gauges after the above measurement, to the stress calculation. Then I compared it to the stress results obtained from the moment measurement.

Horizontal branches of *Sciadopitys verticillata*, *Davidia involucrata*, and *Acer tenuifolium* were also used for this measurement. However, a calculation of the tensile stress at the surface was not undertaken due to a lack of data for the Young’s modulus of lateral branches in these species. Morphological details about the branches of each species are given in Table 1.

Measurement of the stress generated in a branch due to dynamic loads

Stress generated in a branch due to dynamic loads, such as wind, rain, and snow, was measured over a 1-year period using strain gauges. Branches of approximately 30-year-old *F. crenata* and *A. homolepis* of unknown age were used for the measurement. For each species, a lower

horizontal branch was selected. The length of the branch of *F. crenata* was 6 m and the basal diameter was 6.1 cm. The branch of *A. homolepis* was 2 m in length and the basal diameter was 3.1 cm. The trees were growing in small forests and the effects of dynamic loads such as wind and rain were expected to be small. A point near the base (10 cm away) of both branches and a point 100 cm away from the base of the branch of *F. crenata* were selected as measurement points. The strain was measured for the up–down direction at all points [CH-1 (near the base) and CH-3 (100 cm away from the base) for *F. crenata* and at CH-1 for *A. homolepis*] and the right–left direction at the base of the branch for *F. crenata* (CH-2 for *F. crenata*). In late April 2011, the surface of the upper and lower sides of each measurement point and the left and right sides near the base of the branch of *F. crenata* were decorticated at a size of 3 cm × 3 cm. Then strain gauges (FLA-5-11-5LJRA, Tokyo Sokki Kenkyujo Co., Ltd.) were attached to each decorticated surface and connected to the dynamic strain recorder using the method described in Chapter 2. The value of strain was set to show a positive change with a downward deflection of the branch or a negative change with an upward deflection of the branch. Strain data were then recorded for a period of one year.

The accumulated strain data were divided into files of 10,000 successive data points in time order. Then the maximum, minimum, and average were extracted for each file. The difference between the maximum and average of each file was calculated and regarded as the strain due to instantaneous loads (e.g., wind or rain). The variation of the average value was used to detect the deflection due to dynamic loads over longer intervals. Each data was converted into a stress value using equation (5) and the measured Young's modulus data obtained by destructive test. From these data, I determined the maximum stress that was generated in the year due to each dynamic load and calculated the breaking safety factor including all of the stresses that the branch experienced in one year, i.e., the sum of the stress

due to the branch's own weight and the maximum stress value imposed by an instantaneous load.

Statistical analysis

The measurement data were analyzed by multiple regression, and multiple correlation coefficients were calculated by KyPlot version 2.0 beta 15.

3.3. Results

Morphological characteristics of each branch

Six *F. crenata* and seven *A. homolepis* branches obtained from several trees were measured. The basal diameter of each branch ranged from 2 to 6 cm. The length of the branches was 3.0–8.0 m for *F. crenata* and 1.8–5.0 m for *A. homolepis*. The slope at the base was 21.5 ± 12.8º (mean ± SD) in *F. crenata* and 2.7 ± 7.6º in *A. homolepis*. In *F. crenata*, the slope was not horizontal at the base, but was horizontal at the other parts.

Measurement of the mechanical properties of each branch and the moment due to its own weight

The moment at each point along a branch due to the branch's own weight was almost proportional to the cube of the diameter for both species (Fig. 10). This indicates that the effect of the increase in the moment on the tensile stress at the surface is offset by the increase in the diameter at each point along a branch [refer to equation (7)].

The results of the destructive test are shown in Fig. 11. Correlation was hardly observed between the modulus of rupture and the diameter in both species (R = 0.20 for *F. crenata* and R = 0.17 for *A. homolepis*). The average of the modulus of rupture was 55.0 ± 1.0 $MN \cdot m^{-2}$ (mean ± SE) for *F. crenata* and 53.5 ± 2.1 $MN \cdot m^{-2}$ (mean ± SE) for *A. homolepis*. The values of the modulus of rupture in *A. homolepis* were more scattered than those in *F. crenata*.

Young's modulus obtained by destructive testing of each section of the branches was larger in the thin portion than the thicker portion for *F. crenata* (R = –0.66), whereas there was no correlation between Young's modulus and the branch diameter in *A. homolepis* (R = 0.02; Fig. 12). The average Young's modulus was 4.71 $GN \cdot m^{-2}$ for *F. crenata* and 2.21 $GN \cdot m^{-2}$ for *A.*

homolepis. The Young's modulus that was calculated to eliminate shear stress (E/G = 30) averaged 5.37 $GN \cdot m^{-2}$ for *F. crenata* and 2.63 $GN \cdot m^{-2}$ for *A. homolepis*. A negative correlation was found between the diameter and the modified Young's modulus in *F. crenata* (R = –0.45), whereas a weak positive relationship was obtained for *A. homolepis* (R = 0.25). The Young's modulus obtained from the measurement using strain gauges was larger than that obtained by destructive testing.

Calculation of the tensile stress at the surface of the branch

The σ_{sw} values calculated from the moment measurement data are plotted against diameter in Fig. 13. The tensile stress at the surface (σ_{sw}) calculated from the moment measurement data was slightly lower at positions where the diameter was smaller than 2 cm compared to other positions. For positions where the diameter was larger than 2 cm, the range of σ_{sw} values was constant and showed little correlation with diameter (R = 0.086 for *F. crenata* and R = 0.030 for *A. homolepis*). In the individual branches, tensile stress at the surface was largest in the vicinity of the base of branches and gradually decreased toward the tip. The range of σ_{sw} values was 3–20 $MN \cdot m^{-2}$ in *F. crenata* and 3–15 $MN \cdot m^{-2}$ in *A. homolepis*. The average was 9.21 ± 0.28 $MN \cdot m^{-2}$ (mean ± SE) for *F. crenata* and 8.16 ± 0.29 $MN \cdot m^{-2}$ (mean ± SE) for *A. homolepis*.

Calculation of the breaking safety factor

In *F. crenata*, the breaking safety factor was 3–8 for the parts of the branch where the diameter exceeded 2 cm, but was larger in sections with a diameter smaller than 2 cm (Fig. 14). The breaking safety factor of the thin parts of *Fagus* branches varied widely with a range of 4–14. In *A. homolepis*, the breaking safety factor ranged from 4 to 10, with more variation in values than in the thicker parts (ϕ > 2 cm) of the branches of *F. crenata*. The safety factor did not increase in

sections with a diameter smaller than 2 cm in *A. homolepis*, as was observed in *F. crenata*. For individual branches, the safety factor (which was calculated from the stress data based on moment measurements) became larger toward the tip in both species (Fig. 15).

Measurement of strains in branches

The displacement contribution degree of the individual branches became lower toward the tip until a point about 100 cm away from the base of the branch, and became higher toward the tip at portions closer to the tip (Fig. 16). The value was not completely the same between branches, but the style of displacement did not appear to be very different. This result is not inconsistent with the elastic similarity hypothesis.

The tensile stress calculated from the strain due to the liberation of the branches from gravity did not display the above tendency and was almost uniform along the branches, whereas in *F. crenata*, the σ_{sw} value calculated from the strain measurement data was larger at the base of the branches than at other points along the branches (Fig. 15). Strains due to the liberation of the branches from gravity displayed the same tendency in *S. verticillata*, *D. involucrata*, and *A. tenuifolium* (Fig. 17), which is quite different from the distribution of σ_{sw} values calculated from the moment measurements. The stress values calculated from the strain due to the liberation of the branches from gravity using the Young's modulus value from strain gauge measurements were similar to the σ_{sw} values taken from the moment measurements, although those calculated from the strain due to the liberation of the branches from gravity using the Young's modulus value from destructive testing were slightly smaller than those calculated from the moment measurements.

In the experiment that released the growth stress from the branches, some differences were noted between the strains at the upper and lower sides of the branches generated by the cutting

and notching treatment for almost all specimens of *A. homolepis*, *S. verticillata*, and *F. crenata*, and the difference was larger in specimens with a larger diameter (Fig. 18). This indicates that the large values of the strain due to the liberation of the branches from gravity at the base of the branches included a strong element of springback. The actual strain in nature ($\varepsilon_c + \varepsilon_g$) was still larger at the base in some branches of *F. crenata* and most branches of *S. verticillata*, whereas the tendency for a larger value at the base of branches disappeared in most branches of *A. homolepis* when considering the actual strain in nature (Fig. 19).

Measurement of the stress generated in a branch due to dynamic loads

The variations in the average, maximum, and minimum values of the tensile stress of *F. crenata* in the up–down direction are shown in Fig. 21. The average value increased in mid-May and decreased in autumn, probably due to foliation and defoliation, respectively. In winter, the average value sometimes increased rapidly and soon fell to the original value. This variation was due to snowfall. The values of the tensile stress in the right–left direction in *F. crenata* fluctuated irregularly in the range of –10 to 20 (Fig. 22). Generally, the value of the tensile stress due to an instantaneous load was larger in the up–down direction rather than in the right–left direction (Fig. 23).

The maximum of stress due to each dynamic load is shown in Table 2. The stress due to dynamic loads was lower than the stress due to the branch's own weight. The safety factor considering all loads was 3.5 in *F. crenata* and 3.9 in *A. homolepis*, both of which were sufficiently safe.

3.4. Discussion

Measurement of the moment due to the branch's own weight

The fact that the measured values of the moment due to each branch's own weight were proportional to the cube of the diameter (Fig. 10) suggests that the relationship between these two parameters is adjusted so that the tensile stress at the surface of a branch does not vary greatly along a branch. Little correlation existed between the modulus of rupture and the diameter (Fig. 11), which indicates that the larger value of the breaking safety factor in slender portions of branches was due to the small tensile stresses generated by each branch's own weight at these points.

The range in σ_{sw} values obtained from the measurements using the two different methods for *Fagus* and *Abies* branches seemed to overlap each other (Fig. 15). The σ_{sw} calculated from the moment measurement data was largest at the points near the base of the branch and gradually decreased toward the tip, whereas the strain measurement for the liberation of branches from gravity did not display this trend, except for the portions near the base, and the trend for larger values near the base almost disappeared in *A. homolepis* when the elements of growth strain were deducted (Fig. 19). When looking at the strain value, the trend for larger values near the base remained in *F. crenata* and *S. verticillata* even after the deduction of residual strain. However, this was not necessarily true for strain measurements in *F. crenata* because Young's modulus (obtained from the strain gauge measurement) was relatively lower in the vicinity of the base of the branch than in the other portions (Fig. 20). There are still few data of the strain measurement, and there is reformability about the measurement procedure. Because the difference between the values of Young's modulus obtained from the measurement using strain gauges and destructive testing was observed, measuring Young's modulus may be

necessary before measuring the strain due to the branch's own weight and the growth strain, when I calculate stress from the strain measurement. However, from the results presented here, one can consider that the stress due to the branch's own weight in the vicinity of the base of the branch is considerably reduced by growth stress. Considering the effect of growth stress generated by reaction wood, determining the stress state may be difficult by considering only the allometric relationship of the external characteristics in lateral branches.

The breaking safety factor was in a constant range for both species, which suggests that branches are formed so as to maintain safety against bending damage. The safety factor was 3–14 in *F. crenata* and 4–10 in *A. homolepis*, consistent with the description of the breaking safety factor by van Gelder et al. (2006). They found that the value differed significantly among species. However, they also showed that it was similar in shade-tolerant and pioneer species. Evans et al. (2008) reported that the stress σ due to a branch's own weight is relatively constant along a branch and among species (on average about 11 $MN \cdot m^{-2}$) for 40 species, which is also consistent with the results presented here. The values that I recorded varied in the range of 4–10, although measurements were performed on branches under similar wind conditions and photoenvironments. The widest variation in the breaking safety factor was found in the narrow parts of branches, suggesting that narrow parts are not appropriate for comparative studies among several species.

The two species used here for measurements (*F. crenata* and *A. homolepis*) have a different wood structure, especially in their reaction wood, and different Young's modulus values, whereas the safety factor on the basis of their own weight was similar. The environment of the plants used in this study was approximately the same. Therefore, the conclusion can be made that the degree of mechanical safety that a branch requires does not differ greatly between angiosperms and conifers.

Confirmation of the elastic similarity hypothesis

The value of the displacement contribution degree varied little among the individuals. Neither of the two biomechanical hypotheses could be rejected by considering this result and the results for the tensile stress of the branches. The compatibility of the two hypotheses may depend on the branching design of the branch. However, further research is required to determine whether branches design themselves so as to satisfy both hypotheses.

Measurement of the stress generated in a branch due to dynamic loads

The maximum tensile stress due to dynamic loads was lower than the stress due to the branch's own weight, suggesting that the effect of a branch's own weight on branch morphogenesis is considerable for the branches used in this study. Therefore, for considering the uniformity of branch safety against breakage, using the safety factor of branches based on their own weight should be appropriate. The safety factor in consideration of all loads was around 3.5 for *F. crenata* and 3.9 for *A. homolepis*, indicating the branch had a structure that provided considerable safety against breakage due to the dynamic load. (If a branch were located in an environment where it was exposed to a stronger wind than the environment of the branch used in this measurement, the safety factor on the basis of its own weight could be higher than the result above, as observed in a trunk (King 1981).)

The value of the tensile stress due to the instantaneous load was larger in the up–down direction than in the right–left direction (Fig. 23), which indicates that the influence of wind or other dynamic load is stronger in the up–down direction than in the left–right direction. This would be the result of the form of the branch that arranged its twigs and leaves in a horizontal plane. The projected area of the branch from the bottom was apparently larger than from the

side.

A possibility exists that the distribution of the stress along a branch generated by wind or other dynamic load differs from that generated by the branch's own weight. Further measurements are required to investigate this possibility.

4. Tree branching: Leonardo da Vinci's rule versus biomechanical models

4.1. Introduction

Many studies have examined tree design, which has led to several empirical rules. Leonardo da Vinci proposed that the sum of the cross-sectional area of all tree branches above a branching point at any height is equal to the cross-sectional area of the trunk or the branch immediately below the branching point (Richter, 1970). This relationship can also be expressed by stating that the branch cross-sectional area below a given branching node is equal to the sum of the cross-sectional areas of daughter branches above the node (Nikinmaa, 1992; Horn, 2000; Sone et al., 2005; West and Brown, 2005; Sone et al., 2009). This is known as Leonardo da Vinci's rule, or the area-preserving rule (Horn, 2000). However, not all branches correspond to da Vinci's rule. Sone et al. (2005) found that the average yearly growth of the cross-sectional area of a branch was less than the sum of growth of its daughter branches. This is because the proportion of the current-year growth area to the cross-sectional area of the branch is almost always greater in small, young branches than in large, old branches. The authors noted that da Vinci's rule would not hold if the decrease in basipetal growth was repeated every year. Sone et al. (2009) demonstrated that in *Acer rufinerve*, only branches that have experienced shedding follow da Vinci's rule.

One reason for the lack of agreement with da Vinci's rule in some branches may be expressed in terms of their biomechanical structure. About the mechanical limitation, two biomechanical hypotheses, has been already raised in the preceding chapters. In chapter 3, the results were not clearly inconsistent with either hypothesis. However, considering the results in chapter 3 and the report that trunks grown in different mechanical environment have different

slenderness from each other (King, 1981; Meng et al., 2006), it is natural to think that some kind of mechanical limitation acts on branch morphogenesis. Models of branch form which was made based on the two biomechanical hypotheses are called the uniform stress model and the elastic similarity model (McMahon and Kronauer, 1976; Dean and Long, 1986; Bertram, 1989). The allometric relationships for these biomechanical hypotheses may be regarded as a rule for branch tapering. In the biomechanical models, the taper of a branch is expressed by one equation and is assumed to be smooth. However, real branches ramify, and it is reasonable to suppose that the diameter near the ramifying point deviates from the taper equation if biomechanical stress limits branch shape (because the weight that the branch must bear changes dynamically below and above the branching point). Assuming that one of the biomechanical hypotheses applies to tree branch architecture, the diameter needed to maintain the mechanical strength of a branch varies with branching angles and relative weights of distal branches. The relevant question is whether da Vinci's rule is strictly maintained for any realistic branching pattern when either of the biomechanical hypotheses is true. In other words, can da Vinci's rule be applied to biomechanically limited branches? Branches may not conform to da Vinci's rule when the diameter measurement points are restricted to positions that are near the branching point, which may be true for both biomechanical models.

In this study, I calculated the ratio of the cross-sectional areas of the upper and lower sides of a branching point of a branch using the two biomechanical models, and checked whether computed values matched da Vinci's rule. I also took field measurements of this ratio in real branches of *Fagus crenata* and *Abies homolepis* to examine whether da Vinci's rule is strictly maintained, and to check the predictions of the biomechanical models. On the basis of these data, I (i) discuss the question posed above, (ii) determine whether da Vinci's rule is biomechanically adequate, and (iii) determine whether da Vinci's rule is consistent with either

of the two biomechanical models when applied to natural branching patterns.

4.2. Materials and methods

I used the daughter/mother ratio, *i.e.*, the ratio of the total cross-sectional area of the daughter branches to the cross-sectional area of the mother branch at the branching point, as an index for da Vinci's rule. Here, the daughter branches represent parts of a branch after ramification and the mother branch represents the part before ramification. If a tree obeys da Vinci's rule, the daughter/mother ratio must be 1.0 at any branching point of the tree.

Calculation of the daughter/mother ratio using biomechanical models: Is da Vinci's rule consistent with biomechanical models?

A model for the uniform stress hypothesis

In my simulations, I considered a horizontal branch ramifying into *n* daughter branches within a horizontal plane, and calculations were performed for a virtual branch with an *n* of 2 or 3. Branches were assumed to be mostly influenced by their own weight. Each daughter was identified by *i* (*i* = A, B, etc.; Fig. 24). A branch's applied load was assumed to consist only of its own weight, which acts in the direction vertical to the plane in which the branch was arranged. I calculated the diameters of daughter and mother branches at the branching point based on the assumption that branches had a constant safety factor (uniform stress). I then calculated the daughter/mother ratio.

In the model, a branch was regarded as a horizontal beam loaded in the vertical direction. According to material mechanics, the relationship between the diameter and the load that acts on a beam at an arbitrary point can be represented as equation (7) and it can be rewritten as:

$$d = \sqrt[3]{\frac{32M}{\pi\sigma}} \tag{17}$$

where M is the moment determined by the magnitude of the load and the distance from the

loading point. Under the conditions of the uniform stress model, σ is constant, and the diameter depends only on the moment.

The moment that occurs at the branching point of the mother and daughter branches (M_M and M_i, respectively) is

$$M_M = \sum \left(W_i \cdot g_i \cdot \cos\theta_i \right) \tag{18}$$

$$M_i = W_i \cdot g_i \tag{19}$$

where W_i is the weight of daughter i, g_i is the distance between the center of gravity of daughter i and the branching point, and θ_i is the branching angle of daughter i. When calculating the daughter/mother ratio, it is possible to set the measurement points of diameters as the branching point. However, when measuring in the field, there may be some distance between the branching point and the measurement point. Considering this, the moments can be rewritten as

$$M_M = \sum W_i (g_i \cos\theta_i + m_M) \tag{(18)'}$$

$$M_i = W_i (g_i - m_i) \tag{(19)'}$$

where m_M and m_i are distances between the branching point and the measurement point of the mother or daughter i, respectively. In equation ((18)'), the section between the branching point and the measurement point on the mother branch is assumed to have little effect on M_M. I ran the calculation applying zero and some probable values (1, 2, 3, and 5 cm) to m_M and m_i. Substituting equation ((18)') or ((19)') into (17) gives the diameter of the mother and daughters. Applying these diameters, the cross-sectional area of the mother A_M at the branching point can be obtained from

$$A_M = \frac{\pi d_M^2}{4} = \frac{\pi}{4} \left(\frac{32 \sum W_i \left(g_i \cos\theta_i + m_M \right)}{\pi \sigma} \right)^{2/3} \tag{20}$$

where d_M is the diameter of the mother branch. The total cross-sectional area of the daughters

ΣA_i can be obtained from

$$\sum A_i = \frac{\sum \pi d_i^2}{4} = \sum \left(\frac{\pi}{4} \left(\frac{32 W_i (g_i - m_i)}{\pi \sigma} \right)^{2/3} \right) \tag{21}$$

where d_i is the diameter of the daughter i. From equations (20) and (21), the daughter/mother ratio is

$$\frac{\sum A_i}{A_M} = \frac{\sum \{W_i (g_i - m_i)\}^{2/3}}{\{\sum W_i (g_i \cos\theta_i + m_M)\}^{2/3}} \tag{22}$$

According to equation (22), the daughter/mother ratio is independent of the maximum bending stress.

I calculated the daughter/mother ratio for various situations with different branching angles and daughter weights. The angles ranged from 0.1 to 90º and the daughter weights ranged from 1 to 10 kg. In simulations for branches where n equaled 3 (see the following results), the weight of the main daughter branch (as with branch B shown in Fig. 24) was set to 10 kg.

A model for the elastic similarity hypothesis

This model basically follows McMahon and Kronauer (1976). In the elastic similarity hypothesis, the deflection at the tip of a branch is assumed to be proportional to the overall length of the branch (McMahon and Kronauer, 1976). In other words, the deflection angle of an arbitrary microsection of a branch (with the constant relative length) is determined by its relative position on the branch, independent of branch length.

McMahon and Kronauer (1976) assumed that the diameter in the vertical plane at a certain point is proportional to $s^{3/2}$ for a tapered beam, where s is the length of the section of the branch from the (selected) point to the tip. King and Loucks (1978) also referred to the elastic similarity model and explained the relationship between diameter and length of a branch bending under its

own weight as follows: for branches that maintain self-similarity, branch weight W is proportional to d^2l, where l is the length of the branch, since d^2l is proportional to branch volume. The moment arm is proportional to branch length. Therefore,

$$M \propto d^2 l^2 \quad (23) .$$

If a branch is maintained in an elastically similar form, the relationship between curvature and length can be written as

$$r \propto l \quad (24) ,$$

where r is the radius of curvature of the branch at its base. According to the cantilever beam theory (Timoshenko 1955),

$$r \propto d^4 / M \quad (25) ;$$

substituting (25) and (23) into (24), the relationship between diameter and length is

$$d \propto l^{3/2} \quad (26) .$$

In this study, I used the allometric relationships

$$d = k_1 s^{3/2} \quad (27)$$

$$W = k_2 s^4 \quad (28)$$

$$g = k_3 s \quad (29) ,$$

which can be obtained from the above expressions, where k_1, k_2, and k_3 are constants and g is the distance between the center of gravity and the base of the section of the branch.

I now consider a straight horizontal branch without furcation, whose shape is similar to the form described by McMahon and Kronauer (1976). If determination of branch taper follows elastic similarity, the deflection angle of any section of the branch should be strictly maintained. According to cantilever beam theory, the deflection angle of an arbitrary microsection, $d\theta/ds$, is

expressed by the following equation:

$$\frac{d\theta}{ds} = -\frac{M}{EI} \quad (30),$$

where M is the moment due to the weight of the distal part of the branch, E is the modulus of elasticity or Young's modulus, and I is the second moment of area. For a circular cross-section, I is determined as

$$I = \frac{\pi d^4}{64} \quad (31).$$

For η(:=s/λ), where λ is whole length of the branch, the deflection angle of a microsection with a constant relative length is determined by

$$\frac{d\theta}{d\eta} = -\frac{M\lambda}{EI} \quad (32),$$

and the moment that acts on the microsection due to the portion of the branch distal to the section is calculated as

$$M = Wg = k_2 k_3 s^5 \quad (33).$$

Substituting (31), (33), and (27) into (32) gives

$$\frac{d\theta}{d\eta} = -\frac{64 k_2 k_3}{E\pi k_1^4 \eta} \quad (34).$$

Equation (34) supplies information about the dθ/dη value that should be maintained in branches that keep elastic similarity. I propose that dθ/dη is maintained above and below the furcation, whether or not the taper equation is maintained locally around the branching point. If branching is taken into consideration, the moment that acts on the cross-section of the branch varies dramatically before and after furcation but varies smoothly in other positions that have no ramification. Therefore, the diameter should markedly change before and after branching if elastic similarity is maintained and must locally deviate from the taper equation.

Assuming that the distances between the point of diameter measurement and the branching

point are represented by m_M and m_i, I used equation (34) to determine $d\theta/d\eta$ for the microsection of the diameter measurement point on the mother branch. Subsequently, I considered a branch bearing several daughter branches (Fig. 24) and assumed that the longest daughter branch is a part of the main axis of the whole branch that includes the sections above and below the branching point; thus, the length of the longest daughter branch is a part of λ. The moment that occurs at the diameter measurement point on the mother branch (M_M) can be obtained from equation ((18)').

Substituting equations (31) and (34) into (32), setting (s_l+m_M) as s (:=$\eta\lambda$), I obtain d^4 of the mother branch at the branching point required to maintain a constant $d\theta/d\eta$:

$$d_M^4 = \frac{M_M k_1^4 (s_l + m_M)}{k_2 k_3} \quad (35),$$

where s_l is the length of the longest daughter branch. The square root of equation (35) is d_M^2, which can be used for calculating A_M (= $\pi d_M^2/4$).

The sum of the cross-section areas of daughter branches is

$$\sum A_i = \sum \frac{\pi d_i^{\,2}}{4} \quad (36).$$

From equations (36), (35), and (27), setting (s_i-m_i) as s, the daughter/mother ratio is expressed as

$$\frac{\sum A_i}{A_M} = \frac{\sum \frac{\pi}{4} k_1^2 (s_i - m_i)^3}{\frac{\pi}{4}\sqrt{\frac{k_1^4 M_M (s_l + m_M)}{k_2 k_3}}} \quad (37),$$

where s_i is the length of each daughter branch. Substituting equations ((18)'), (28), and (29), equation (37) can be arranged as

$$\frac{\sum A_i}{A_M} = \frac{\sum \frac{\pi}{4} k_1^2 (s_i - m_i)^3}{\frac{\pi}{4}\sqrt{\frac{k_1^4 (s_l + m_M)\sum k_2 {s_i}^4 (k_3 s_i \cos\theta_i + m_M)}{k_2 k_3}}} = \frac{\sqrt{k_3}\sum (s_i - m_i)^3}{\sqrt{(s_l + m_M)\sum \{s_i^4 (k_3 s_i \cos\theta_i + m_M)\}}} \quad (38) .$$

Using equation (38), I calculated a daughter/mother ratio for a virtual horizontal branch with various branching forms. For k_3, I used the value obtained from the allometric regression equation expressing the relationship between the data for branch length and the distance between the center of gravity of the branch and the branching point for *F. crenata* and *A. homolepis*. These empirical data were obtained by methods described in the following section. If k_3 is constant for any branch form, the daughter/mother ratio varies according to the length and branching angles of lateral daughters.

Field measurements and evaluation of da Vinci's rule and each of the biomechanical models

Data on the diameters of several sections of branches, the lengths of the parts distal to these sections, the distances between the centers of gravity of the distal parts and the measurement section, and the moment due to each of the branch weights at each section were collected in the field measurement described in chapter 3. With these data, I explored the relationships between the length and the distance of the center of gravity of the distal part from the measurement section for each species, using exponential regressions. I used the least-squares method to fit the curves. The equations for the regression curves were used in the above model calculations.

I also collected data on the diameters of mother and daughter branches, the daughters' branching angles, and the number of daughters ramified from a mother branch, using other lower branches of *Fagus crenata* (*ca*. 30 years old) and *Abies homolepis* (age unknown)

specimens growing in the Nikko Botanical Garden (Nikko, Tochigi, Japan, E139°37', N36°45', mean annual temperature = 12.1ºC, mean annual precipitation = 2400 mm); twigs were arranged in a horizontal plane. Thirteen branches from six *F. crenata* trees and 13 branches from seven *A. homolepis* trees were measured. The heights of the sampled *F. crenata* trees and *A. homolepis* trees ranged from 14.1 to 16.9 m (14.7 ± 1.3 m, mean ± SD) and 9.4 to 22.6 m (13.8 ± 5.5 m), respectively. The mean diameters at breast height were 26.4 ± 1.5 cm and 31.6 ± 13.1 cm, respectively. The average height at which the branches attached to the trunks was 1.5 ± 0.4 m for *F. crenata* and 1.6 ± 0.4 m for *A. homolepis*. The length of the branches ranged from 1.8 to 6.3 m (3.2 ± 1.4 m) for *F. crenata* and from 1.1 to 4.5 m (2.1 ± 0.1 m) for *A. homolepis*. The slope at the basal section of the *F. crenata* branches was 30.5 ± 15.0º, which tended to become immediately gentle toward the tip along the branch, so that the slope of the measured section was 20.6 ± 15.3º. For *A. homolepis*, the slope at the basal section of the branches was 14.7 ± 7.8º with little variation along each branch. Several branching points (1–14 per branch) were measured on each branch. Diameters were measured both in the horizontal and vertical planes for each point. The maximum and minimum values of the diameter of mother branches were 56.0 and 8.3 mm for *F. crenata*, and 49.1 and 6.0 mm for *A. homolepis*, respectively. The cross-sectional area for each point was then calculated as an ellipse and as a circle with a diameter obtained in the vertical plane. The ratio between the diameter in the vertical plane and the diameter in the horizontal plane was 1.065 ± 0.007 for *F. crenata* and 1.034 ± 0.003 for *A. homolepis*. The average, maximum, and minimum values of the ratio between the cross-sectional area calculated as an ellipse and the area calculated as a circle with its diameter in the vertical plane were 0.943 ± 0.006 (mean ± SE), 1.140, and 0.785 for *F. crenata*, and 0.970 ± 0.003, 1.105, and 0.803 for *A. homolepis*, respectively. I selected lower horizontal branches because this type of branch ramifies within a horizontal plane, as with the mechanical models

above, simplifying the calculation for the biomechanical validity of branches. The daughter/mother ratio for each branching point was then calculated. The branches were located within a forest, and thus the effects of wind force were expected to be relatively small. The number of daughter branches ramified from a mother was always 2 in *F. crenata* and 2–5 in *A. homolepis*. I measured 34 branching points for *F. crenata* and 39, 37, and 3 branching points in *A. homolepis* with 2, 3, and more than 4 daughters, respectively. Branching points were weaker than other sections, and therefore thicker. I chose a measurement point located where the thicker section ended. As a result, the measurement points were 1–8 cm away from the branching point, despite our efforts to minimize the distance between branching and measurement points. The larger the mother branch, the larger the required distance was between the measurement point and the branching point. The effect of this distance was assumed to be negligible because the distance was small compared with the overall size of the branches.

The above biomechanical model calculations refer to the difference between the weight of the main branch and the lateral daughters. Therefore, an index that defines the weight difference between the daughters is required for analysis of the measured data. I defined this difference as the daughters' degree of deviation and described it as

$$\frac{\left(\frac{W_l}{\sum W_i}\right)-\frac{1}{n}}{\left(\frac{n-1}{n}\right)} \quad (39),$$

where W_l is the weight of the largest daughter branch and n is the number of daughters ramified from one mother branch. The numerator indicates the difference between the ratio of the weight of the largest daughter branch to the total weight of the daughter branches (the value of which is restricted into $1/n$; 1 because it is the value related to the largest daughter branch) and the ratio for the situation in which all daughter branches have the same weight, which, in effect,

represents the extent of deviation from the uniformity of the weight of daughter branches. This value can vary from zero to (*n*-1)/*n*. It was standardized by dividing by (*n*-1)/*n* so that the upper limit of the value of the daughters' degree of deviation becomes 1.0. Therefore, the daughters' degree of deviation has the following characteristics. When one of the daughter branches is much larger than the others, the degree approaches 1. When a branch does not ramify, *i.e.*, the weights of the other branches are zero, the value is 1. In contrast, when there is no difference between the weights of daughter branches, the degree is zero. The weight of each daughter branch was determined from the regression equation already calculated from field data.

The validity of the uniform stress model was also examined. If a branch obeys the uniform stress model, the relationship between daughter and mother branches can be determined as follows. According to the uniform stress model, the relationship between the moment and diameter at any point on a branch is described by equation (17). Combining equations (18), (19), and (17), the relationship between the diameter of the mother branch and the diameters of daughter branches is

$$d_M^3 = \frac{32M_M}{\pi\sigma} = \frac{32\left(\sum M_i \cos\theta_i\right)}{\pi\sigma} = \frac{32\left(\sum \left(d_i^3 \pi\sigma/32\right)\cos\theta_i\right)}{\pi\sigma} = \sum\left(d_i^3 \cos\theta_i\right) \quad (40) .$$

From this, $\sum(d_i^3\cos\theta_i) / d_M^3 = 1$ is expected if the maximum bending stress is constant along the branch. I used the left side of this equation as an index for the uniform stress model and examined the validity of the elastic similarity model using the following equation, derived from equations ((18)'), (30), and (31):

$$\frac{\sum\left(d_l/d_i\right)^{2/3} d_i^4 \cos\theta_i}{d_M^4} = 1 \quad (41) .$$

The left side of equation (41) was used as the index for the elastic similarity model. For simplicity, the distance between the branching point and the measurement point was not considered in these calculations.

I performed statistical analyses to assess the relationship between the cross-sectional area of the mother branch and the sum of the cross-sectional areas of the daughter branches, the relationship between the daughters' degree of deviation and the daughter/mother ratio, and the relationship between the daughters' degree of deviation and the index for each of the biomechanical models. Correlation coefficients were calculated for these relationships with MS Excel 2010 (Microsoft Corporation). Linear regressions were also performed using the least-squares method for each relationship.

Using the data on diameter and branching angle of each daughter branch, I also estimated daughter/mother ratios, assuming that the branches follow one of the two mechanical models. If a branch were to follow the uniform stress model, the daughter/mother ratio would be calculated using equation (22). Assuming that a branch obeys the elastic similarity model, the daughter/mother ratio can also be calculated using the equation derived from equations (38) and (27). For simplicity, I describe the equation for which m_{i} and m_{M} are zero, resulting in

$$\frac{\sum A_i}{A_M} = \frac{\sum {d_i}^2}{\sqrt{{d_l}^{2/3} \sum \left({d_i}^{10/3} \cos\theta_i \right)}} \qquad (42) .$$

Subsequently, I compared each of the estimated daughter/mother ratios with the actual daughter/mother ratio using the method proposed by Kozak and Smith (1993). A measure of mean bias, B ($= \sum \left(Y_i - \hat{Y}_i \right) / n_{\mathrm{o}}$), and the standard error of estimation, SEE $= \sqrt{\sum \left(Y_i - \hat{Y}_i \right)^2 / \left(n_{\mathrm{o}} - k \right)}$, were calculated for each model, where Y_{i} is the actual observation of the dependent variable, $\hat{Y}_i$ is the predicted value of the actual observation, n_{o} is the number of observations, k is the number of estimated parameters used in the estimation, and $\overline{Y}$ is the average of the actual observations. For completeness and to determine the magnitude of the effects of m_{i} and m_{M}, I also calculated the daughter/mother ratio for each biomechanical model

with equations (22) or (38), using the actual m_i and m_M values, and applied the allometric relationships between diameter and length, between diameter and the distance from the base to the center of gravity, and between diameters and weights of branches and k_3 (all obtained from the branch group that excluded those branches used for determining daughter/mother ratios). I also determined the daughter/mother ratio excluding the bark in an indirect manner, using the relationship between diameter and bark thickness obtained from the branch group that excluded branches used for determining daughter/mother ratios. The daughter/mother ratio obtained in this indirect manner is less reliable than other measures because it includes several indirect elements. Nevertheless, the rough estimates proved useful in our considerations of magnitudes of effects.

4.3. Results

Differences in daughter/mother ratios between each of the biomechanical models and da Vinci's rule, estimated by model calculations

After applying various values to the branching angles and weights of daughter branches, using the uniform stress model, I found that the daughter/mother ratio was always > 1.0 if m_M and m_i were assumed to be zero. However, the daughter/mother ratio generally decreased when m_M and m_i were set to larger values. The daughter/mother ratio increased when the weights of the lateral daughter branches (which grow in different directions relative to the mother branch) relative to the weight of the main daughter branch (which has a branching angle of zero) increased (Fig. 25, Fig. 26, Table 3, Table 4 and Table 5). This tendency was amplified when lateral daughter branching angles were increased (Fig. 27, Fig. 28). This occurred because the daughter/mother ratio also increased with the branching angles of lateral daughter branches, as the moment of the mother branch was influenced by the cosine of each daughter's branching angle.

For any ratio of the total lateral daughters' weights and the main daughter's weight, the minimum value of the daughter/mother ratio can be found when the branching angles of the daughters are near zero (Fig. 25, Fig. 26). The larger the weight of the main daughter relative to that of the lateral daughters is, the lower the minimum value of the daughter/mother ratio is. For example, when the number of daughter branches was 2 (and one of them was the main daughter) and m_M and m_i were assumed to be 1.0, the minimum value of the ratio was 1.24 for W_A:W_B = 1:1.When the ratio between the main and the lateral daughters was 10:1, the minimum daughter/mother ratio fell to 1.04, which can be treated as roughly equal to 1 (Fig. 25A and Table 3). When assuming a branch with two daughters and neither of them was a main daughter, the ratio was larger than the above values (Fig. 25B and Table 4). When the weights of the branches were fixed, the daughter/mother ratio rose with increasing daughter branching angles;

gently in the range of 0–60º, and swiftly in the range of 80–90º (Fig. 25B).

When the number of daughters was three or more, the value of the daughter/mother ratio was generally larger than the above values calculated for the branching points with one main daughter and one lateral daughter (Fig. 26, Table 5). In Fig. 26, the daughters consisted of one main daughter and several lateral daughters. However, it is also possible to have no main daughter. In such a situation, the daughter/mother ratio should be larger because the rate of the moment that the mother branch must bear, originating from lateral daughter branches (reduced by the cosine effect), is larger than when a branch has a main daughter.

It should be noted that values may be overestimated when there is poor balance with respect to the mother axis between daughter branches A and B or between daughter branches A and C (e.g., the upper left corner of Fig. 25B because the actual branch must bear the shear stress due to torsion. If the daughters are balanced or the main daughter is sufficiently heavier than other daughters, the shear stress is likely to be negligible. In reality, branches that have extremely unbalanced daughter branches were rarely observed and therefore, this would not be a serious problem for branches in nature.

The constants needed for elastic similarity model calculations obtained from field measurements were $k_2 = 4.91 \times 10^{-11}$ and $k_3 = 0.3932$ for *F. crenata* and $k_2 = 3.93 \times 10^{-10}$ and $k_3 = 0.4397$ for *A. homolepis*. The change in the value of the daughter/mother ratio obtained from the elastic similarity model calculations using these values was similar to that obtained from the uniform stress model (Fig. 27, Fig. 28, Table 6, Table 7 and Table 8). However, the absolute value of the daughter/mother ratio obtained from the elastic similarity model was larger under the same conditions for a branch with three daughters. The daughter/mother ratio generally decreased when m_M and m_i were set to large values, whereas the trend mentioned above was maintained when m_M and m_i were set to large values or changed by the same method as that

used for the measurement point choice I established in my field observations. Estimated values for the elastic similarity model might also deviate from the actual value due to shear stress when there is poor balance with respect to the mother axis between the daughter branches A and B or daughter branches A and C.

Comparison between actual and theoretical values of the daughter/mother ratio; validation of the biomechanical models in F. crenata and A. homolepis

The sum of the cross-sectional areas of daughter branches was a little larger than the cross-sectional area of the mother branch at most branching points in *F. crenata* and at some branching points in *A. homolepis*, whereas the daughter/mother ratios were not so much away from 1.0 (Fig. 29). The daughter/mother ratio for these branching points became larger as the daughters' degree of deviation became smaller, but this trend was very weak for branching points with two daughters in *A. homolepis*, and the value was very close to the value obtained when using da Vinci's rule for branching points with two daughters in *A. homolepis* (Fig. 29, Table 3). This tendency for negative correlation did not change whether the cross-sectional area was calculated as an ellipse or a circle, and appeared to roughly coincide with the two biomechanical model predictions rather than with da Vinci's rule. Indeed, $\sum (d_i^3 \cos\theta_i) / d_M^3$, the index used for the uniform stress model, was almost 1.0 (0.97 ± 0.02 SE), regardless of the daughters' degree of deviation in *F. crenata* (Fig. 30A, r = 0.06). Thus, the stress uniformity seems to explain the branch form near branching points in *F. crenata*. However, in *A. homolepis*, the value of the index deviated somewhat from the theoretical value (0.88 ± 0.02; Fig. 30B). Here, contrary to our expectations, $\sum (d_i^3 \cos\theta_i) / d_M^3$ increased with increasing daughters' degree of deviation in *A. homolepis* (Fig. 30B, Table 3).Therefore, the uniform stress model does not apply well to the branching points of *A. homolepis* branches. A difference in the trend of the

daughter/mother ratio among the groups of branching points with different number of daughter branches (*n*) was observed. In *A. homolepis*, the slope of the relationship between the daughter/mother ratio and the daughters' degree of deviation increased with *n*. On the other hand, the slope of $\sum (d_i^3 \cos\theta_i) / d_M^3$ decreased with *n*.

The index for the elastic similarity model became smaller than 1.0 as the daughters' degree of deviation neared zero and generally took on a value smaller than the index for the uniform stress model in both species (Fig. 31, Table 9), therefore deviating more from the theoretical value than the uniform stress model. In *F. crenata*, there appeared to be little correlation between the index for the elastic similarity model and the daughters' degree of deviation (average: 0.88 ± 0.03, mean ± SE). However, in *A. homolepis*, there was a positive correlation between these variables, particularly in branches with two daughters; this was also the case for the uniform stress model index (Table 3). These results indicate that the uniform stress model represented real branches in *F. crenata*, but neither the mechanical models nor da Vinci's rule represented *A. homolepis* branches.

Statistical analyses of predicted and measured daughter/mother ratios showed that the measured ratio was smaller than the predicted ratio in both mechanical models and was larger than the value obtained with da Vinci's rule (=1; Table 10). Analyses also showed that SEE was smallest for the uniform stress model in *F. crenata* and for branching points with three or more daughters in *A. homolepis* (the measured daughter/mother ratio value was nearest to the prediction of the uniform stress model in *F. crenata* and for branching points with three or more daughters in *A. homolepis*). However, for branching points with two daughters in *A. homolepis*, SEE was smallest for the value obtained with da Vinci's rule. Thus, I suggest that branches in *F. crenata* and branching points with three or more daughters in *A. homolepis* comply with the uniform stress model, whereas branching points with two daughters in *A. homolepis* comply

with da Vinci's rule. When excluding bark thickness, the daughter/mother ratio for *F. crenata* became slightly larger, but our conclusions remained almost unaffected. As an exception, the exclusion of bark thickness in *A. homolepis* from the daughter/mother ratio decreased the value (it approached 1.0 in both branching points with two daughters and branching points with three or more daughters) and decreased SEE for da Vinci's rule (Table 10). Therefore, it is possible that branching points with three daughters in *A. homolepis* best comply with da Vinci's rule. For branching points with four or more daughters in *A. homolepis*, SEE (excluding bark thickness) was smallest in the elastic similarity model, indicating the possibility that these branching points best comply with the elastic similarity model. The daughter/mother ratios calculated by the biomechanical models from the measured diameters of daughter branches when including m_i and m_M were slightly smaller than the ratios calculated without them (in both species), but the difference was very small and did not change our conclusions.

4.4. Discussion

From the biomechanical model calculations, I demonstrated that the daughter/mother ratio is influenced by differences among daughter weights and branching angles and may deviate from 1.0 when the weights or branching angles of lateral daughter branches are relatively large (when mechanical limitations dominate tree design). For a common branching occurrence in nature where the main daughter is much larger than lateral daughters, the ratio may be close to 1.0. In such a case, the maintenance of mechanical stability or safety may keep the value near 1.0, resulting in agreement with da Vinci's rule. The daughter/mother ratio value can also be close to 1.0 when the lateral daughters' branching angles are small. In practice, the angles are 50–80º for *A. homolepis* and 10–50º for *F. crenata*. These values are sufficient (i) to produce a bending point such that the daughter/mother ratio is far more than 1.0 and (ii) for determining whether branching points best fit da Vinci's rule or one of the biomechanical models.

In *F. crenata* field measurements, diameters measured at points before and after branching were in agreement with the uniform stress model. The elastic similarity model was less congruent with empirical measurements, but the indices of both models were close to 1.0. This indicates that horizontal branches of *F. crenata* fit the uniform stress model best, the elastic similarity model second, and da Vinci's rule least well. The results in the chapter 3 also provide good support for the uniform stress model. However, for *A. homolepis*, the daughter/mother ratio closely followed da Vinci's rule for branching points with two daughters. In this species, indices of the two models changed with the daughters' degree of deviation, contrary to our expectations. Furthermore, the daughter/mother ratio estimated without bark followed da Vinci's rule better for branching points with two or three daughters, although the increasing trend with decreasing daughters' degree of deviation was minimal for branching points with three daughters. Thus, it seems that the architecture of *A. homolepis* branches near branching points is

forced to maintain a positive da Vinci's rule index rather than to conform to biomechanical safety or stability. However, the stress variations along branches caused by the branches' own weights were minimal in *A. homolepis*, other than in segments close to the proximal end, indicating that branches of this species maintain uniformity of mechanical safety (chapter 3). A possible explanation for this contradiction in *A. homolepis* may be the heterogeneity of wood properties. The relationship between maximum bending stress and diameter at a point on a branch may vary with the mechanical properties of wood. Reaction wood (tension wood and compression wood) is produced in inclined trunks, and differs from normal wood in mechanical properties. The theoretical values I calculated assumed that the wood was uniform in its properties. It is possible that the reaction wood content in branches influenced their mechanical properties and diameters; under these circumstances, there may be simultaneous compliance with da Vinci's rule and a uniformity of stress. Additionally, branch shedding may also have affected results. In young *A. homolepis* branches, the number of daughters ramifying from one mother branch was usually three and sometimes four or more, and branching points with two daughters may have experienced cladoptosis. Sone et al. (2009) showed that only branches that have experienced shedding coincide with da Vinci's rule in *Acer rufinerve* and suggested that shedding is necessary to maintain da Vinci's rule in branching architecture. Such a branch may have established its architecture according to mechanical constraints before shedding, at which time it did not coincide with da Vinci's rule, and then shed several daughter branches of a certain cross-sectional area so that the branch diameters temporarily would coincide with da Vinci's rule. The diameters of such branches may be modified gradually if mechanical constraints exist, and there may be many branches in various states of modification in nature. Thus, it seems natural that a scattering of index values will occur after cladoptosis. However, without bark, the estimated daughter/mother ratio fit da Vinci's rule well, for most branching

points. Therefore, it is reasonable to suppose that a branch of *A. homolepis* will comply with da Vinci's rule regardless of the number of daughter branches.

The uniform stress model predicted the daughter/mother ratio better than the elastic similarity model in both species. Therefore, I propose that the branches I measured were more consistent with the uniform stress hypothesis than with the elastic similarity hypothesis.

Da Vinci's rule does not define the locations at which cross-sectional areas should be measured. The daughter/mother ratio measured at points nearest the branching point often deviated from 1.0, but the deviation was moderate and the ratio could be 1.0 if measurements were made farther from the branching point. The daughter/mother ratios calculated by the biomechanical models followed the same trend, and similar ratio values were predicted. Thus, Leonardo da Vinci's rule does not rule out compliance with biomechanical models in realistic circumstances. Similarly, the models do not preclude compliance with da Vinci's rule, although predictions of the two models and da Vinci's rule are not identical.

The method used here can also be applied to branches that are not horizontal, and can be modified to include the mechanical stress caused by wind, provided that the displacement of the branch is negligible. Indeed, the mechanical stress due to dynamic loads such as wind and snow is an important factor in a tree's mechanical safety (Niklas, 2000; Niklas and Spatz, 2000; Dean et al., 2002). The biomechanical calculations can be applied to any branch form by decomposing the load acting on the branch, whatever the cause, into three-dimensional elements (two vertical and one horizontal). Further verification of various branch shapes requires additional data on the mechanical state of branches in nature.

I did not investigate tree branching in terms of hydraulic ability which is also a possible factor limiting tree morphology in this study. Further studies are required to clarify the relationship between hydraulic ability and tree branching.

5. General discussion

The studies described in chapter 2 and 3 reevaluated the two biomechanical models that were established as a branch form that mechanical support is adequately materialized.

In the study of the mechanical property of trunk form, the wind load-generated surface stress on the trunk of an isolated *Larix kaempferi* tree was smaller in the lower portion of the tree than in the upper portion. The safety of the trunk was sufficiently reliable to tolerate wind speeds more than twice as large as the maximum wind that actually blew in Nikko City even at the most weak portion. Also for branches, it was suggested that enough mechanical safety exists to protect against the actual mechanical environment. Therefore, it seems that tree trunks and branches produce their shapes to be safe in intact conditions. It may be the time when remarkably intense wind blows or a remarkably large quantity of snow falls, or when the wood is rotten from the inside and the strength of the trunk or branch have decayed that the destruction happens.

In the study of horizontal branches, the result that the uniformity of the stress was generally kept and the distribution of the degree of deflection along the branch was similar among the branches led to the conclusion that both mechanical hypotheses (the uniform stress model and the elastic similarity model) could apply to real branches. To answer the question of why the both mechanical hypotheses can be applied to real branches, a simulation using a branching model and the analysis of growth stress inside the branches will be needed. The equation of the power function of the branch taper in consideration of the ramifications may be different from the equation considering a branch without ramifications. Taking the measurement data of the bending safety factor into consideration, the difference in the range of breaking safety factors among the different diameter situations should not be ignored. Since breaking safety factor took

a wider range of values in thinner portions of the branches, such portions are not appropriate when the difference of breaking safety factor among several species is examined.

In the tree trunk, higher positions were more susceptible to the wind force than the basal position. This result suggests that it is necessary to think about priority—which part is needed or which part may be shed or lost—from the view point of survival strategy of individual trees when considering tree biomechanics, rather than only assuming the lean form in terms of breakage. This is the case not only for the trunk, but also for the whole plant, including lateral branches. To evaluate the elastic similarity hypothesis for tree trunks, it is necessary to analyze the information found in the literature and record further data. (However, it may still be quite difficult to evaluate the hypothesis with respect to the tree trunks.) For lateral branches, the portion near the fixed end was weak, at least in terms of the self-weight. Or if I reflect on my crude result on growth stress, a weak part that was common to all branches did not seem to exist. I think the latter finding means that not only is the position along a branch where it might break not a fixed position, but that a part that is not the main body of the branch may be risky. The yielding of branches often happens at the fixed end as if scooping out a part of the trunk. Therefore, I think that the fixed end of the branch is the weak point. Structures with weak fixed ends may be convenient for branches that may be dropped during the plant's growth.

Tree form varies according to the growth environment. A problem that remains to be settled is how the mechanical safety of a branch is changed by the environment surrounding the branch. Depending on the environment, it may be necessary to change the tactics with mechanical aspect for branch. Tree form is limited by more than mechanics. Photoenvironment has the biggest influence on how the branches should be arranged since plants grow branches to capture light. Mechanical limitation of the branches is only a supporting factor in tree morphology, and we must not forget that the tree will do what is necessary for efficient photosynthesis. However,

continuing observation of tree form from a mechanical point of view may help to explain even inexplicable phenomena, only if one considers the placement of the leaves in a manner that is advantageous to photosynthesis. In addition, it may be necessary to pay attention to water transportation. There are several studies that have referred to the hydraulic limitations of tree form (Ryan and Yoder, 1997; Niklas and Spatz, 2004; Ryan et al., 2006). The water transferability may be the firm limit that acts on the tree form in dry environments. I think it is necessary to study tree form comprehensively by adding these elements other than biomechanics in the future.

Finally, I propose other future research prospects. First, I intend to study the relationship between the form and mechanical state or properties of branches that extend in the diagonal direction. The direction of each load that acts on the non-horizontal branches may be different from that of horizontal branches. If we can elucidate the relationship between the angle of inclination and mechanical state of branches, we may be able to better understand economic branch arrangement in a plant. The inhomogeneity of the wood in branches is also interesting. The disproportionate growth stress generated by including reaction wood produces a positive effect on the direction decision of the branch. I intend to clarify how much reaction wood is included and generates growth stress in branches of various angles and forms. I would further like to investigate the extent of its effect on branch formation cost. Studies about the difference of wood properties in different sections of a branch are also needed. Additionally, I intend to apply the method of measurement of mechanical states or properties of branches to a comparative study among individual trees growing in different environments or among a variety of species. This may theoretically explain the survival strategies among species or within a species when growing in different environments.

6. Tables

Table 1. Morphological traits of the branches in each species.

Table 1 Morphological traits of the branches of each species

	Length (m)	Basal diameter (mm)	Basal slope (°)	Age
Coniferous				
Abies homolepis	1.8 - 5.0	22 - 57	8 - 13	20 - 34
Sciadopitys verticillata	2.9 - 4.1	34 - 58	-8 - 0	---
Broad-leaved				
Fagus crenata	3 – 6	35 - 58	---	15 - 23
Davidia involucrate	3.3 - 4.2	22 - 29	4 - 27	---
Acer tenuifolium	4.0	42	24	---

Table 2. Maximum tensile stress due to each load and the safety factor considering all loads.

Table 2 Maximum tensile stress due to each load

	Fagus crenata	*Abies homolepis*
Type of load	Maximum value of stress (kg/cm^2)	
Self-weight (July or August)	88.3	85.8
Instantaneous load (wind, rain, etc.)	71	54.6
Snow	50	33
Foliation	~20	(43~45)
Modulus of rupture	561	545
Safety factor considering all kinds of loads	3.5	3.9

Table 3. Numerical data of Fig. 25A.

	Weight of daughter A (kg)										
θ_A (degrees, θ_B = 0)	**0**	**1**	**2**	**3**	**4**	**5**	**6**	**7**	**8**	**9**	**10**
0	1.00	1.04	1.09	1.13	1.17	1.20	1.22	1.24	1.25	1.26	1.26
10	1.00	1.04	1.09	1.13	1.17	1.20	1.23	1.25	1.26	1.26	1.26
20	1.00	1.04	1.09	1.14	1.18	1.21	1.24	1.26	1.27	1.28	1.28
30	1.00	1.04	1.09	1.14	1.18	1.22	1.25	1.28	1.30	1.31	1.32
40	1.00	1.04	1.09	1.15	1.20	1.24	1.28	1.31	1.33	1.35	1.37
50	1.00	1.04	1.10	1.15	1.21	1.26	1.31	1.35	1.38	1.41	1.43
60	1.00	1.04	1.10	1.16	1.23	1.29	1.35	1.40	1.45	1.49	1.52
70	1.00	1.04	1.10	1.17	1.25	1.32	1.39	1.46	1.52	1.58	1.64
80	1.00	1.04	1.11	1.19	1.27	1.35	1.44	1.53	1.62	1.71	1.79
90	1.00	1.04	1.11	1.20	1.29	1.39	1.50	1.62	1.74	1.86	2.00

Table 4. Numerical data of Fig. 25B.

	Weight of daughter A (kg)										
θ_A (degrees, $=\theta_B$)	**0**	**1**	**2**	**3**	**4**	**5**	**6**	**7**	**8**	**9**	**10**
0	1.00	1.04	1.09	1.13	1.17	1.20	1.22	1.24	1.25	1.26	1.26
10	1.01	1.05	1.10	1.14	1.18	1.21	1.24	1.25	1.26	1.27	1.27
20	1.04	1.08	1.13	1.18	1.22	1.25	1.28	1.29	1.30	1.31	1.31
30	1.10	1.14	1.19	1.25	1.29	1.32	1.35	1.37	1.38	1.38	1.38
40	1.19	1.24	1.30	1.35	1.40	1.43	1.46	1.48	1.49	1.50	1.50
50	1.34	1.39	1.46	1.52	1.57	1.61	1.64	1.67	1.68	1.69	1.69
60	1.58	1.65	1.72	1.79	1.86	1.91	1.94	1.97	1.98	1.99	2.00
70	2.04	2.12	2.22	2.31	2.39	2.45	2.50	2.53	2.55	2.57	2.57
80	3.20	3.32	3.47	3.62	3.74	3.84	3.92	3.97	4.00	4.02	4.03
90	95.08	93.28	93.95	95.77	98.29	101.29	104.62	108.19	111.94	115.82	119.79

Table 5. Numerical data of Fig. 26.

	Weight of lateral daughters (kg, W_A=W_C)										
θ_A (degrees, =θ_C)	**0**	**1**	**2**	**3**	**4**	**5**	**6**	**7**	**8**	**9**	**10**
0	0.97	1.04	1.13	1.21	1.27	1.32	1.35	1.37	1.38	1.39	1.39
10	0.97	1.05	1.13	1.21	1.28	1.32	1.36	1.38	1.39	1.40	1.40
20	0.97	1.05	1.14	1.22	1.29	1.34	1.37	1.40	1.42	1.43	1.43
30	0.97	1.05	1.14	1.23	1.30	1.36	1.40	1.43	1.46	1.47	1.48
40	0.97	1.05	1.15	1.24	1.32	1.39	1.45	1.49	1.52	1.54	1.56
50	0.97	1.05	1.15	1.26	1.35	1.43	1.50	1.56	1.60	1.64	1.66
60	0.97	1.05	1.16	1.28	1.39	1.49	1.57	1.65	1.72	1.77	1.81
70	0.97	1.05	1.17	1.30	1.43	1.55	1.67	1.77	1.87	1.95	2.03
80	0.97	1.06	1.18	1.32	1.47	1.63	1.78	1.93	2.08	2.21	2.34
90	0.97	1.06	1.19	1.35	1.53	1.72	1.92	2.14	2.36	2.60	2.84

Table 6. Numerical data of Fig. 27A.

	Weight of daughter A (kg)										
θ_A (degrees, θ_B = 0)	**0**	**1**	**2**	**3**	**4**	**5**	**6**	**7**	**8**	**9**	**10**
0	0.99	1.13	1.20	1.26	1.29	1.32	1.34	1.36	1.38	1.39	1.40
10	0.99	1.13	1.21	1.26	1.30	1.32	1.35	1.37	1.38	1.39	1.40
20	0.99	1.13	1.21	1.26	1.30	1.33	1.36	1.38	1.39	1.41	1.42
30	0.99	1.14	1.21	1.27	1.31	1.35	1.38	1.40	1.42	1.43	1.45
40	0.99	1.14	1.22	1.28	1.33	1.37	1.40	1.43	1.45	1.47	1.49
50	0.99	1.14	1.23	1.30	1.35	1.40	1.43	1.47	1.50	1.52	1.54
60	0.99	1.15	1.24	1.32	1.38	1.43	1.48	1.52	1.55	1.58	1.61
70	0.99	1.15	1.25	1.34	1.41	1.47	1.53	1.58	1.62	1.67	1.70
80	0.99	1.16	1.27	1.36	1.44	1.52	1.59	1.65	1.71	1.77	1.82
90	0.99	1.16	1.28	1.39	1.48	1.57	1.66	1.74	1.82	1.90	1.97

Table 7. Numerical data of Fig. 27B.

	Weight of daughter A (kg)										
θ_A (degrees, $=\theta_B$)	**0**	**1**	**2**	**3**	**4**	**5**	**6**	**7**	**8**	**9**	**10**
0	0.99	1.13	1.20	1.26	1.29	1.32	1.34	1.36	1.38	1.39	1.40
10	1.00	1.14	1.21	1.27	1.30	1.33	1.35	1.37	1.39	1.40	1.41
20	1.02	1.17	1.24	1.29	1.33	1.36	1.39	1.40	1.42	1.43	1.44
30	1.06	1.22	1.29	1.35	1.39	1.42	1.44	1.46	1.48	1.49	1.50
40	1.13	1.29	1.38	1.43	1.48	1.51	1.53	1.55	1.57	1.58	1.60
50	1.23	1.41	1.50	1.56	1.61	1.65	1.67	1.70	1.71	1.73	1.74
60	1.39	1.60	1.70	1.77	1.82	1.86	1.90	1.92	1.94	1.96	1.97
70	1.68	1.92	2.05	2.13	2.20	2.25	2.29	2.32	2.34	2.36	2.38
80	2.34	2.68	2.85	2.97	3.06	3.13	3.18	3.22	3.26	3.29	3.31
90	13.13	14.74	15.56	16.17	16.67	17.09	17.45	17.77	18.06	18.33	18.57

Table 8. Numerical data of Fig. 28.

	Weight of lateral daughters (kg, $W_A=W_C$)										
θ_A (degrees, $=\theta_C$)	**0**	**1**	**2**	**3**	**4**	**5**	**6**	**7**	**8**	**9**	**10**
0	0.99	1.27	1.40	1.49	1.55	1.59	1.63	1.66	1.68	1.70	1.71
10	0.99	1.27	1.40	1.49	1.55	1.60	1.63	1.66	1.69	1.70	1.72
20	0.99	1.27	1.41	1.50	1.57	1.62	1.65	1.68	1.71	1.73	1.75
30	0.99	1.28	1.42	1.52	1.59	1.64	1.69	1.72	1.75	1.77	1.79
40	0.99	1.28	1.44	1.54	1.62	1.69	1.73	1.78	1.81	1.84	1.86
50	0.99	1.29	1.46	1.58	1.67	1.74	1.80	1.85	1.89	1.93	1.96
60	0.99	1.30	1.48	1.62	1.72	1.81	1.89	1.95	2.00	2.05	2.09
70	0.99	1.31	1.51	1.66	1.79	1.90	2.00	2.08	2.15	2.22	2.28
80	0.99	1.32	1.54	1.72	1.88	2.02	2.14	2.26	2.36	2.46	2.55
90	0.99	1.34	1.58	1.78	1.98	2.16	2.33	2.49	2.65	2.80	2.95

Table 9. Constants of the regression equations ($y = Ax + B$) and correlation coefficients (r) in Fig. 29, Fig. 30, and Fig. 31.

	Daughter/mother ratio			Index of uniform stress model			Index of elastic similarity model		
	A	**B**	**r**	**A**	**B**	**r**	**A**	**B**	**r**
Fagus crenata									
two daughters	-0.19	1.27	-0.59	0.03	0.96	0.06	0.19	0.79	0.39
Abies homolepis									
two daughters	-0.11	1.16	-0.32	0.41	0.65	0.65	0.64	0.48	0.69
three daughters	-0.43	1.44	-0.81	0.30	0.70	0.58	0.48	0.53	0.67
four or more	-0.23	1.33	-0.42	0.21	0.67	0.64	0.41	0.45	0.78

x represents the daughters' degree of deviation, and y represents the daughter/mother ratio or the index of each biomechanical model.

Table 10. Biases and standard errors of estimates (SEE) of daughter/mother ratios estimated in compliance with the assumptions of each model.

	da Vinci's rule		Uniform stress model		Elastic similarity model	
	Bias	**SEE**	**Bias**	**SEE**	**Bias**	**SEE**
F. crenata						
two daughters	0.180 (0.143)	0.206 (0.178)	-0.072 (-0.062)	0.120 (0.123)	-0.134 (-0.090)	0.183 (0.165)
A. homolepis						
two daughters	0.114 (0.040)	0.159 (0.113)	-0.118 (-0.156)	0.295 (0.252)	-0.176 (-0.109)	0.279 (0.237)
three daughters	0.168 (0.028)	0.216 (0.102)	-0.108 (-0.212)	0.160 (0.274)	-0.160 (-0.106)	0.232 (0.197)
four or more	0.216 (0.059)	0.324 (0.149)	-0.130 (-0.227)	0.168 (0.286)	-0.170 (-0.084)	0.224 (0.126)
Total	0.141 (0.037)	0.190 (0.110)	-0.119 (-0.182)	0.251 (0.259)	-0.177 (-0.113)	0.271 (0.229)

Values in parentheses are estimates obtained from calculations that take m_i and m_M into consideration for the uniform stress model and elastic similarity model, and take bark thickness into consideration for da Vinci's rule.

7. Figures

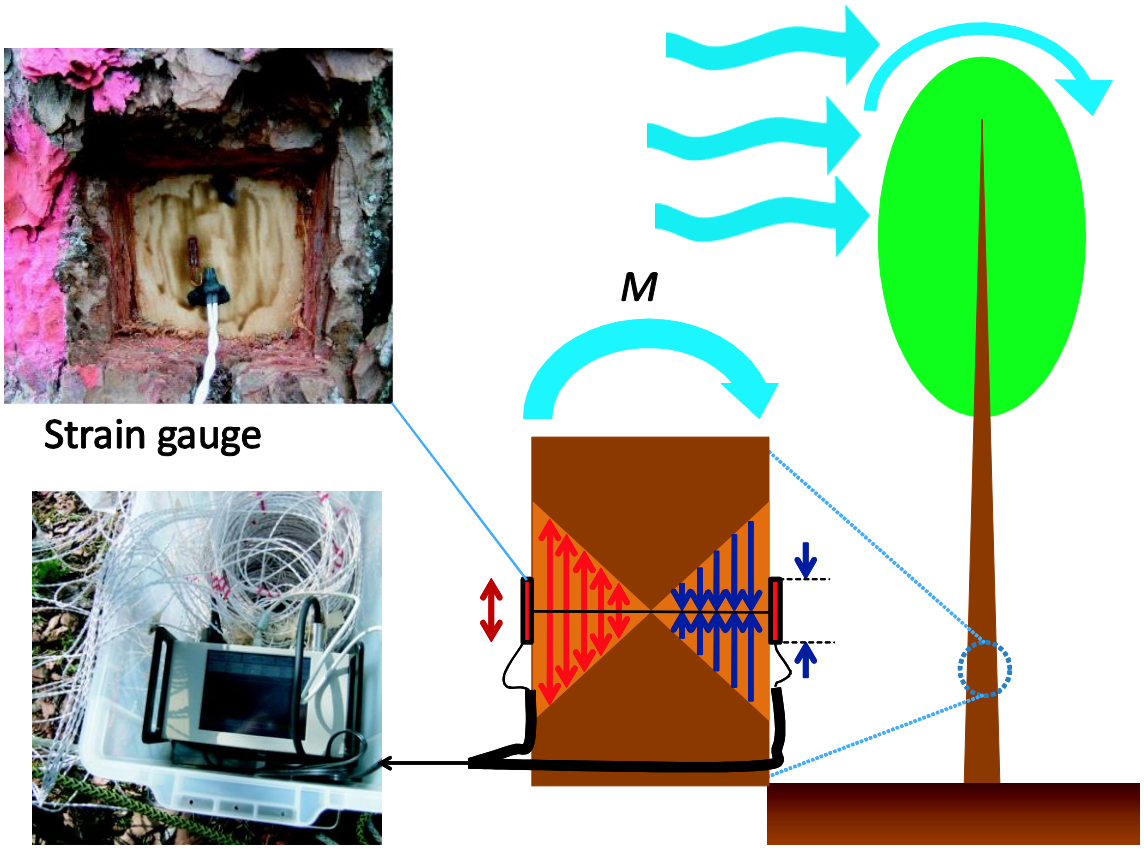

Fig. 1. Strain gauges attached to the barked surface of *Larix kaempferi*.

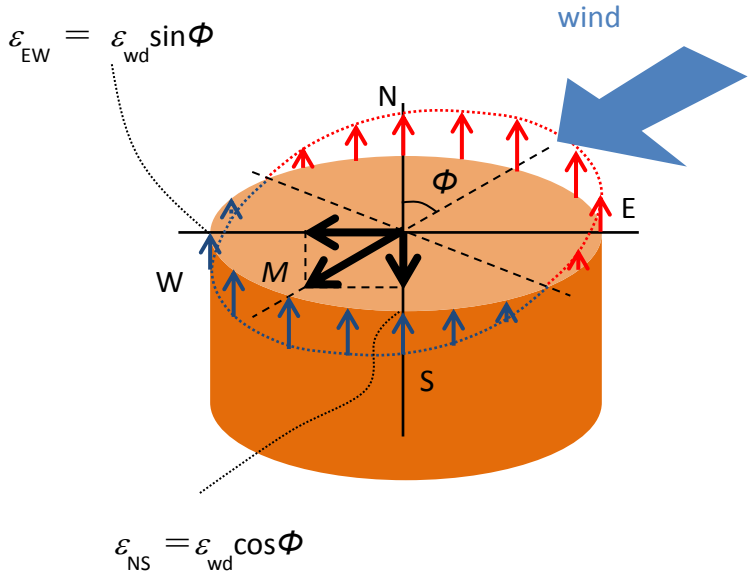

Fig. 2 Relationship between ε_{wd} and ε_{EW} or ε_{NS}. *M* is the bending moment due to the force of the wind.

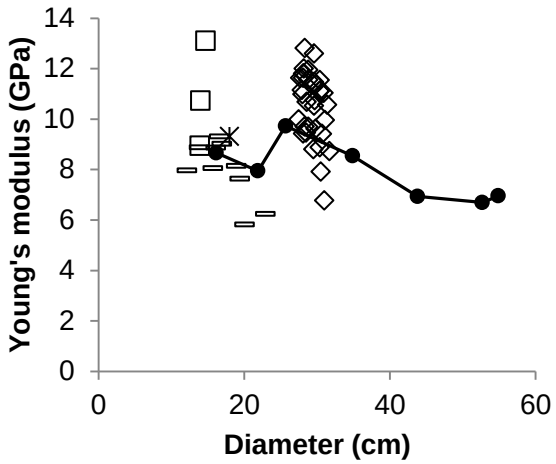

Fig. 3. Young's moduli at various diameters on the trunk of *Larix kaempferi*. The plot with the straight line is for the results of this study. The larger diameter corresponds to the part which is nearer to the base. Other plots (open shapes) are the published Young's moduli of green logs (with bark) of *Larix kaempferi* (Yamamoto et al., 1992; Koizumi and Ueda, 1987; Yoneda, 1987; Yoshino et al., 2010). Each symbol represents the data quoted from each different literature.

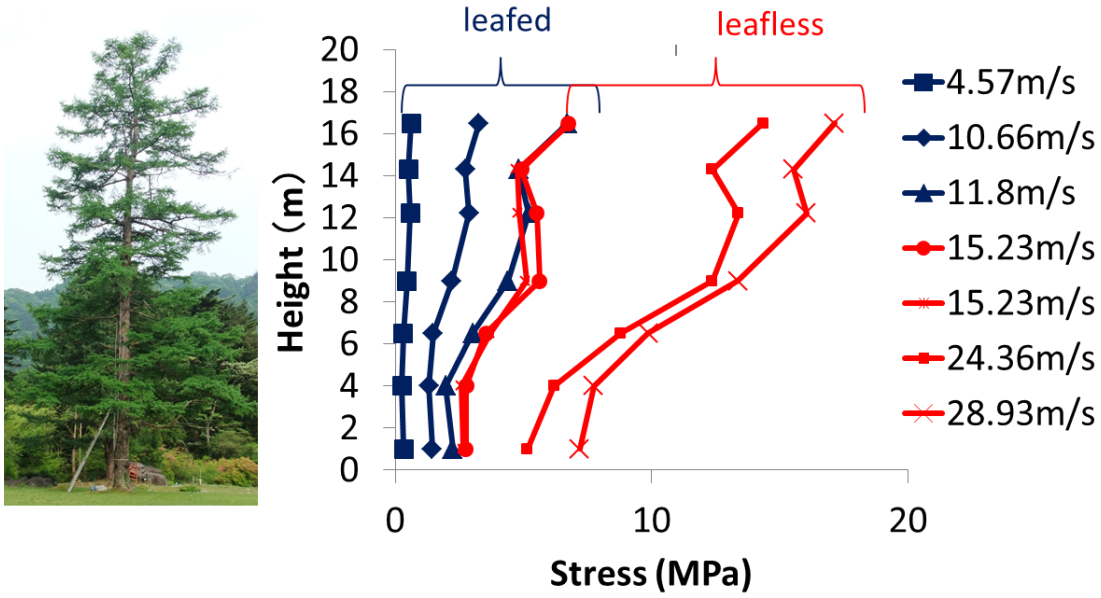

Fig. 4. Stress at the surface along the trunk of *Larix kaempferi* generated by the force of the wind. The data on the graph are important parts picked up from enormous measurement data. Blue lines represent the stresses that occurred when branches had leaves, and red lines represent the stresses that occurred after defoliation. The date of measurement of each data was July 11, 2012, 8:40 a.m. (4.19 m/s), May 16, 2012, 5:06 a.m. (9.14 m/s), July 17, 2012, 6:13 p.m. (10.66 m/s), November 27, 2012, 11:25 a.m. (15.23 m/s), November 27, 2012, 1:05 a.m. (15.23 m/s), February 3, 2013, 5:52 a.m. (24.36 m/s), March 10, 2013, 4:10 p.m. (28.93 m/s), respectively.

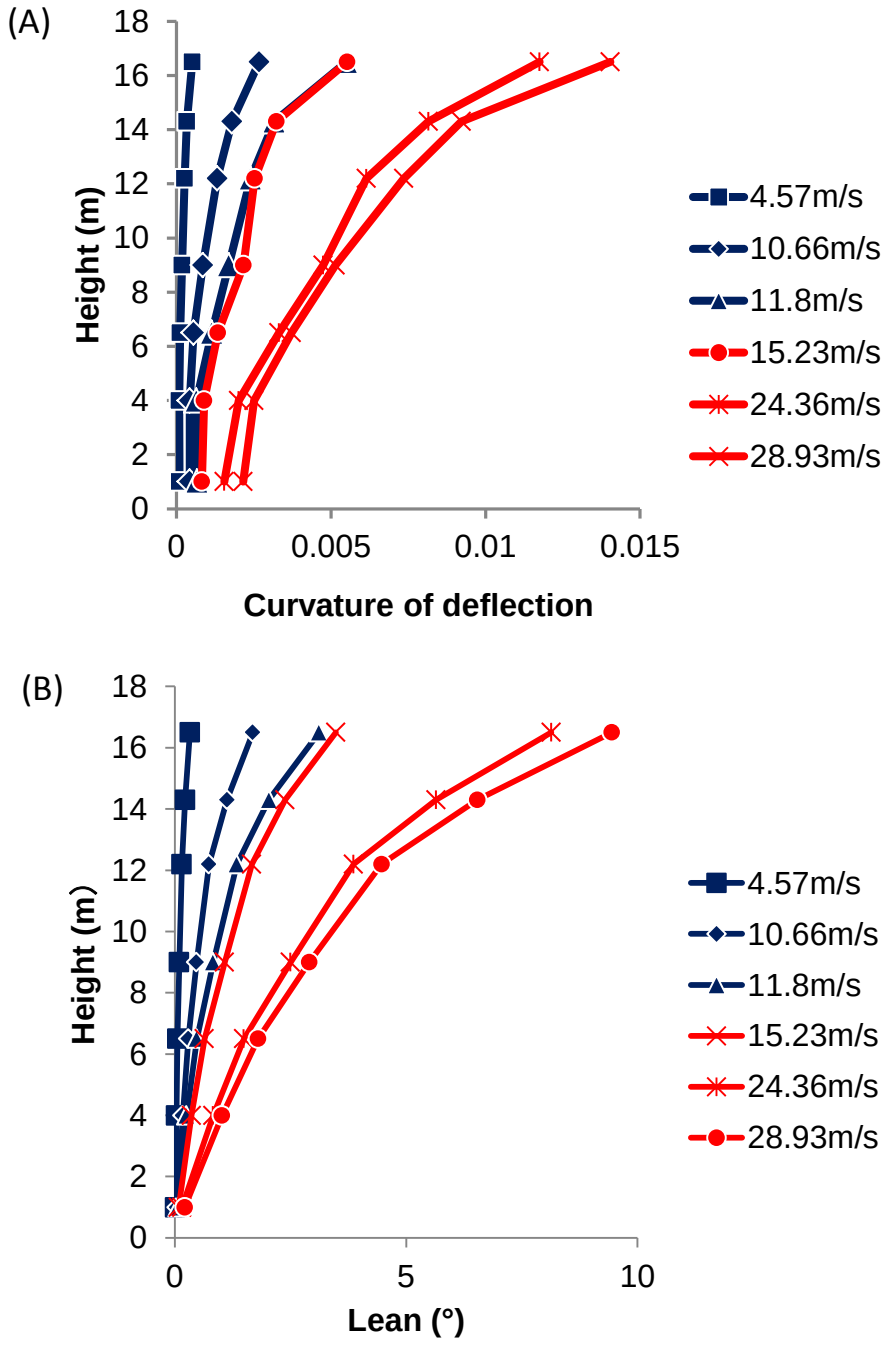

Fig. 5. (A) The curvature of deflection of each minute section to which strain gauges were attached, and (B) the lean of each part of the trunk of *Larix kaempferi* generated by the force of the wind. The curvature of deflection represents the deflection of the 5-mm-long section to which strain gauges were attached. The lean was calculated as the sum of the curvature of deflection of each section of the trunk. Blue lines represent the data obtained when branches had leaves, and red lines represent the data obtained after defoliation.

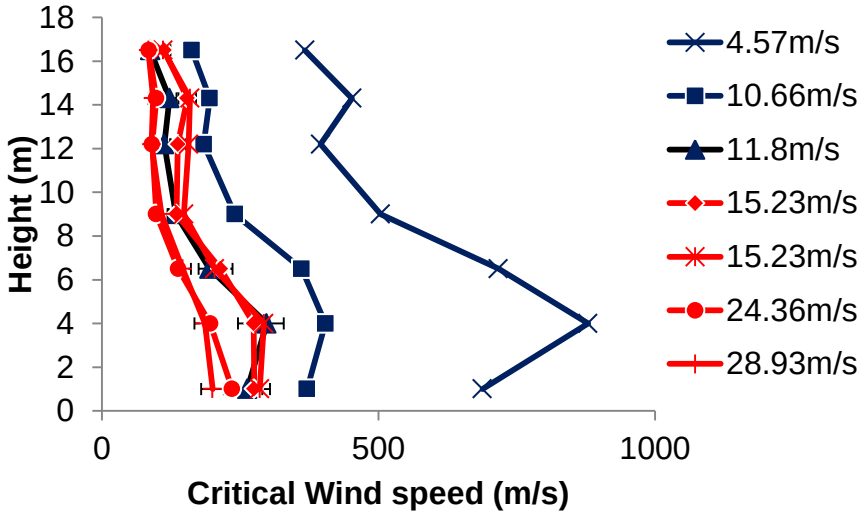

Fig. 6. The critical wind speed at each point along the trunk.

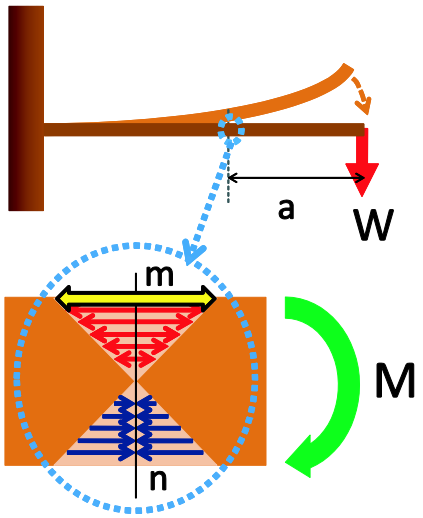

Fig. 7. Schematic diagram of a branch to which a concentrated load is applied. The distribution of internal stress is displayed in the enlarged side view. *a*, the distance from the load point; *M*, moment (= $W \times a$); *W*, load.

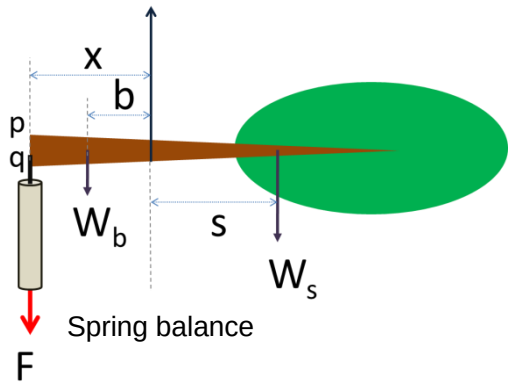

Fig. 8. Diagram of the measurement of the moment that acts on cross section *pq* due to the branch's own weight. *F*, the pulling force at the cutoff point; *b* and *s*, the lengths between the center of gravity of W_b or W_s, respectively, and the suspension point; *x*, the distance between the cutoff point and the suspension point; *W*, the weight of the branch portion distal to the cutoff point; W_b and W_s, the weights of the portion of the branch proximal or distal to the suspension point.

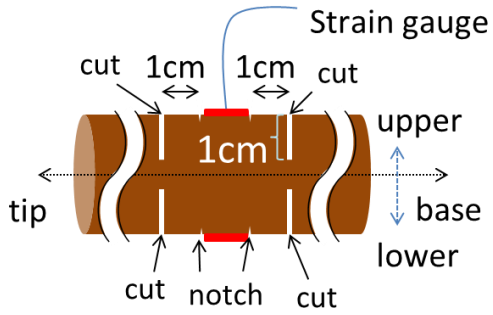

Fig. 9. Illustration of the growth stress liberation procedure.

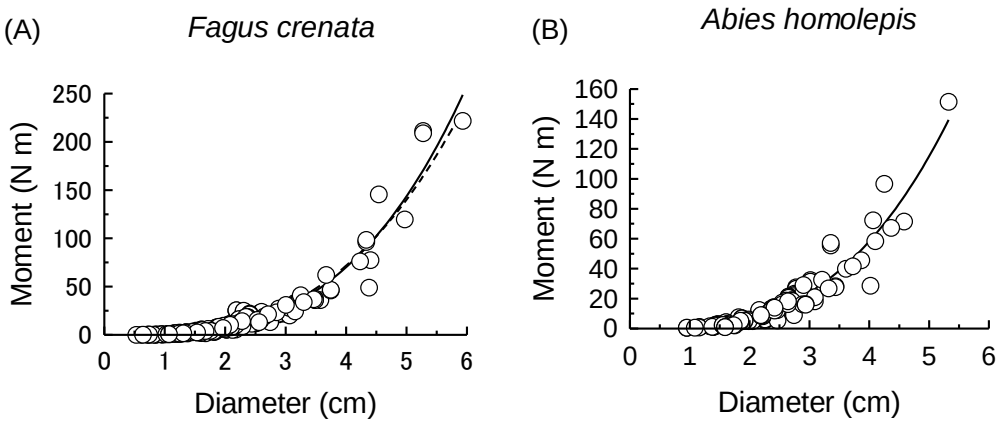

Fig. 10. Relationship between the diameter and the moment due to the weight of a branch in (A) *F. crenata* and (B) *A. homolepis*. The regression curves are drawn based on multiple linear regression. In the left figure, the solid line shows the regression curve of $y = 0.812x^{3.22}$, and the broken line indicates the regression curve of $y = 1.121x^{3}$. In the right figure, the solid line represents the regression curve of $y = 0.850x^{3.05}$.

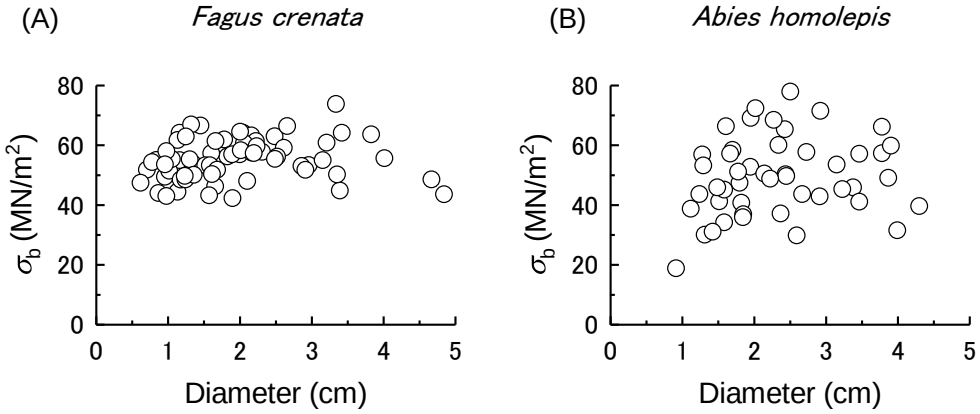

Fig. 11. σ_b plotted against the diameter of branches of (A) *F. crenata* and (B) *A. homolepis*.

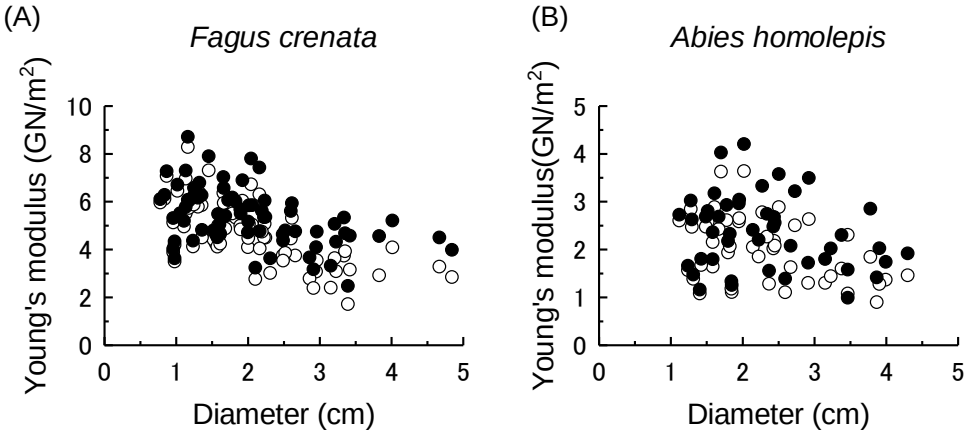

Fig. 12. Young's modulus of each section of the branches of (A) *F. crenata* and (B) *A. homolepis*. Open circles represent the unmodified value of the measured Young's modulus. Filled circles represent the modified Young's modulus assuming that E/G = 30.

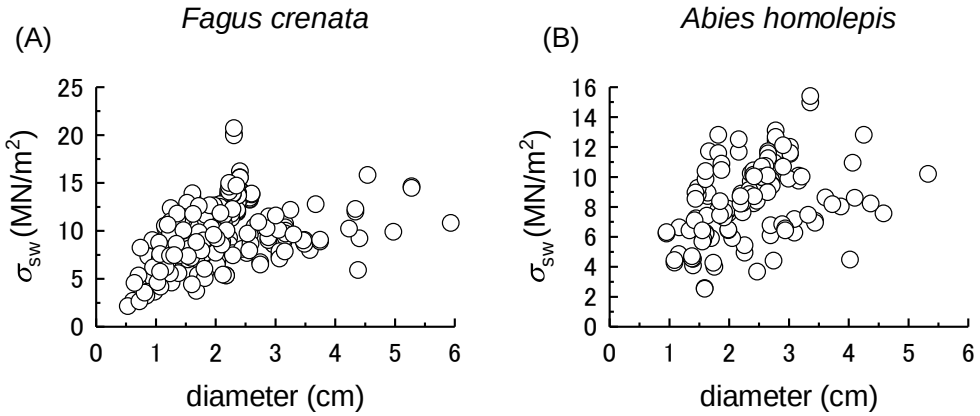

Fig. 13. σ_{sw} due to the branch's own weight calculated from the moment measurement data plotted against the diameter of branches of (A) *F. crenata* and (B) *A. homolepis*.

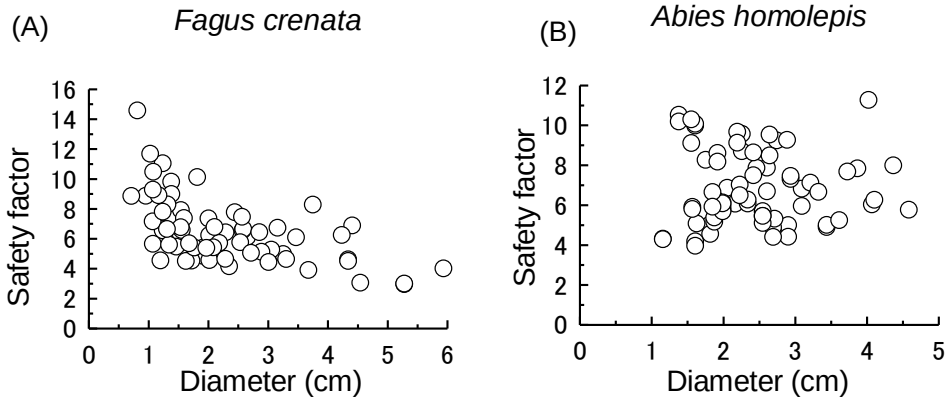

Fig. 14. Breaking safety factors of the lateral horizontal branches of (A) *F. crenata* and (B) *A. homolepis* plotted against diameter.

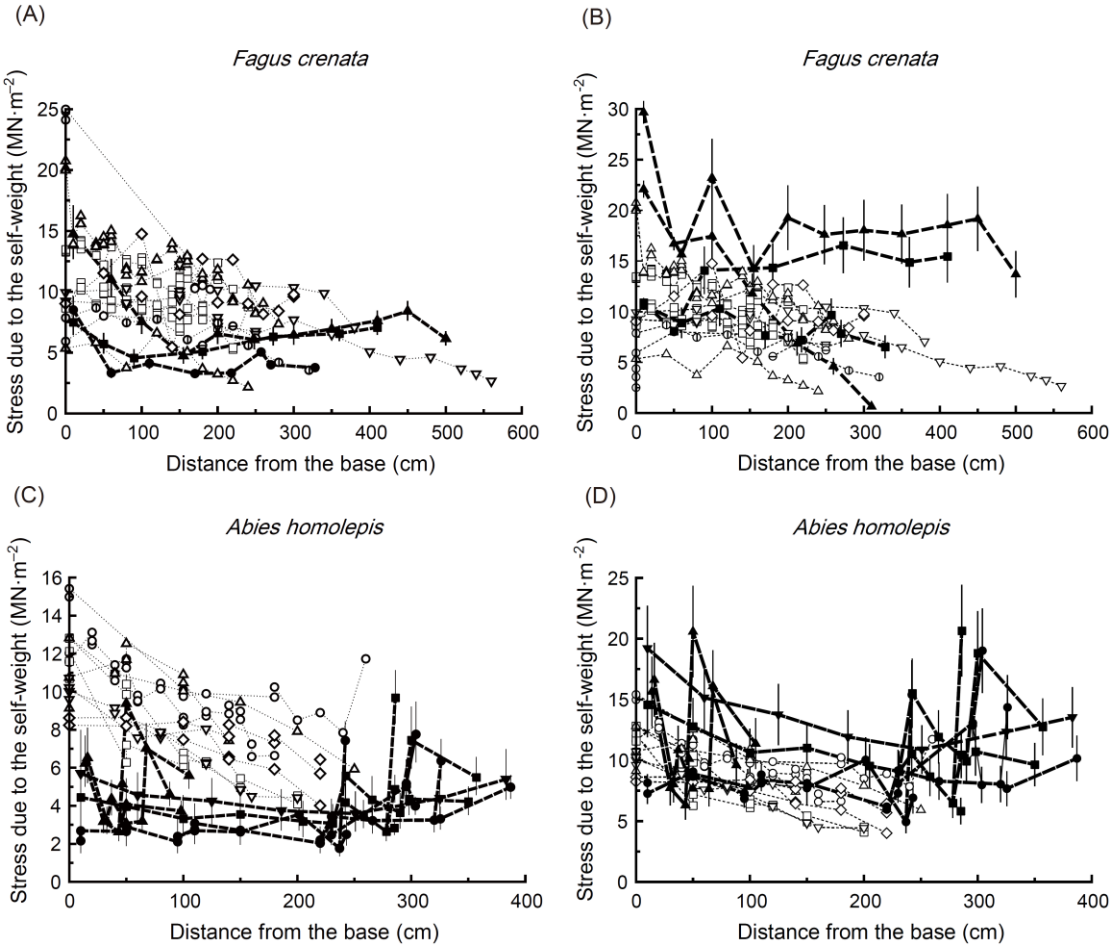

Fig. 15. Stress due to a branch's own weight (σ_{sw}) in (A, B) *F. crenata* and (C, D) *A. homolepis*. The plots with filled symbols connected by dashed lines show the stresses calculated from the strain data and Young's moduli estimated from the data shown in Fig. 12 (A, C) or from the data obtained from the strain gauge measurements (B, D). The plots with open symbols connected by dotted lines show the stress data calculated from the measurement of the moments. The same symbols represent the same branch.

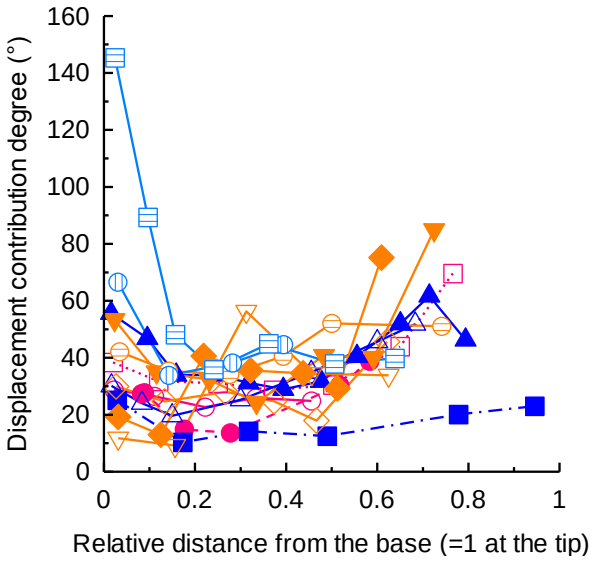

Fig. 16. Displacement contribution degree of each minute segment of the branches plotted against the distance from the base of the branches. Blue, pink, sky blue, and orange symbols represent *F. crenata*, *A. homolepis*, *D. involucrata* and *S. verticillata*, respectively.

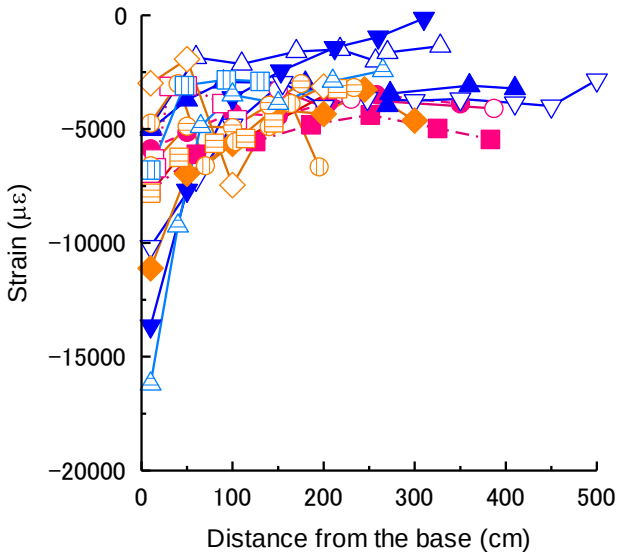

Fig. 17. Strain (the difference between the upper and lower surface) due to the liberation of the branches from gravity in *F. crenata* (blue), *A. homolepis* (pink), *S. verticillata* (sky blue), and *D. involucrate* (orange).

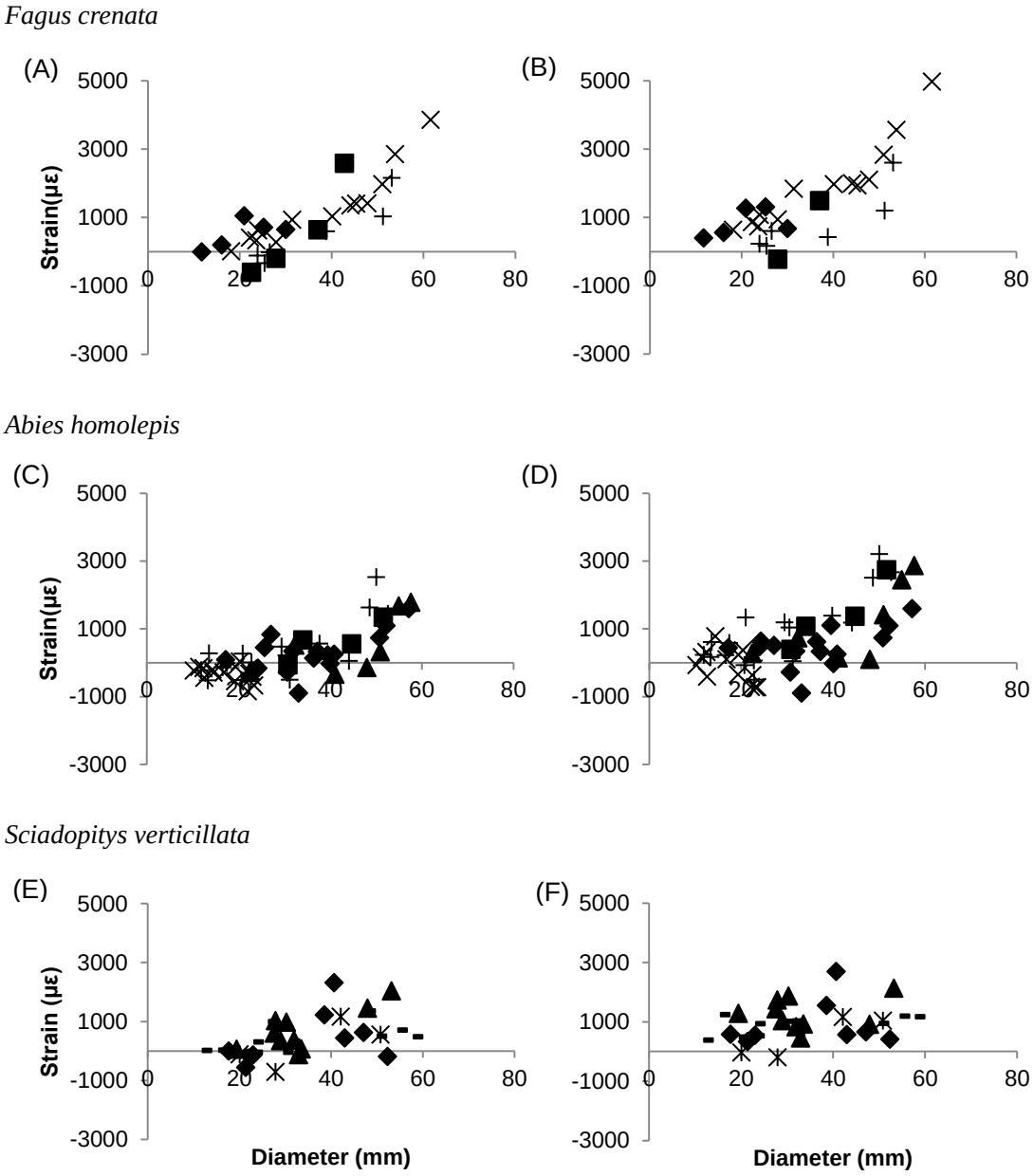

Fig. 18. Residual strain (the difference between the upper and lower surface) obtained by (A, C, E) the cutting treatment or (B, D, F) cutting + notching treatment for (A, B) *F. crenata*, (C, D) *A. homolepis*, and (E, F) *S. verticillata*.

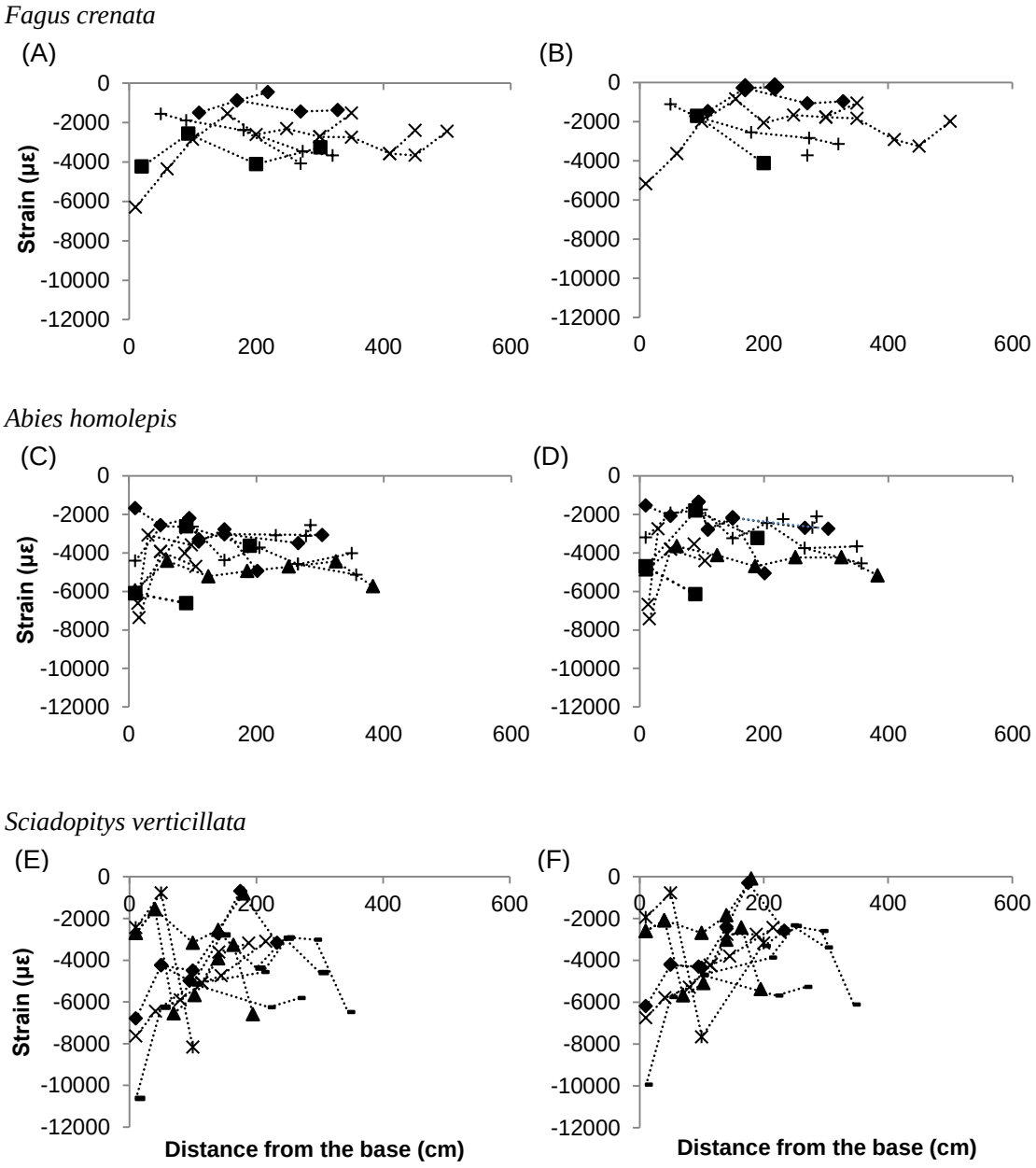

Fig. 19. The modified strain [i.e., the strain value that add the strain generated by the liberation from gravity to the strain obtained by (A, C, E) cutting or (B, D, F) cutting + notching; i.e., the probable actual strain in nature ($\varepsilon_c + \varepsilon_g$)] for the branches of (A, B) *F. crenata*, (C, D) *A. homolepis*, and (E, F) *S. verticillata*.

(A) *Fagus crenata*

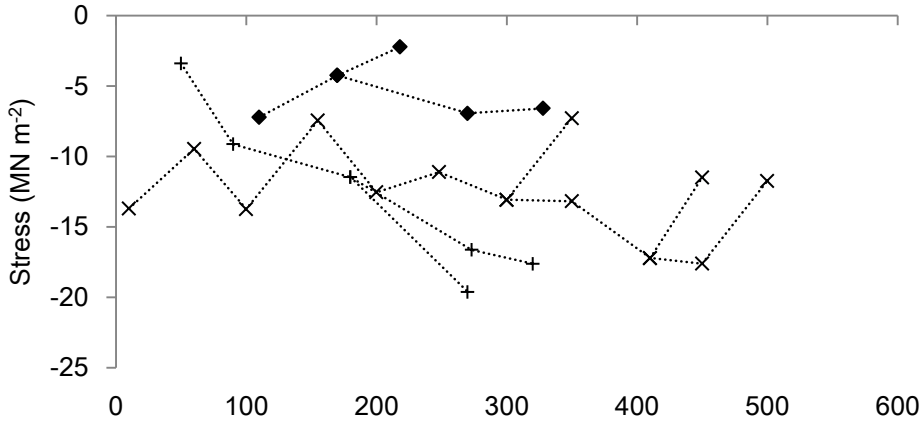

(B) *Abies homolepis*

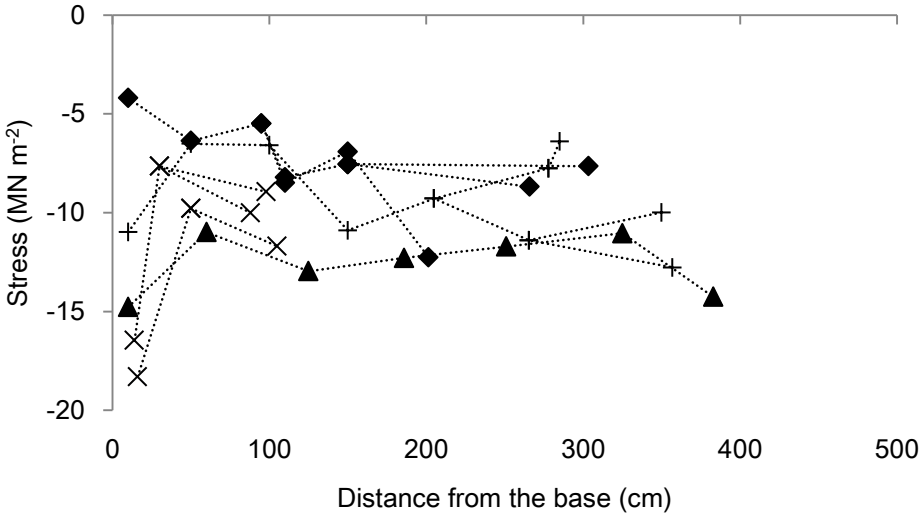

Fig. 20. The modified tensile stress calculated from the modified strain for the branches of (A) *F. crenata* and (B) *A. homolepis*.

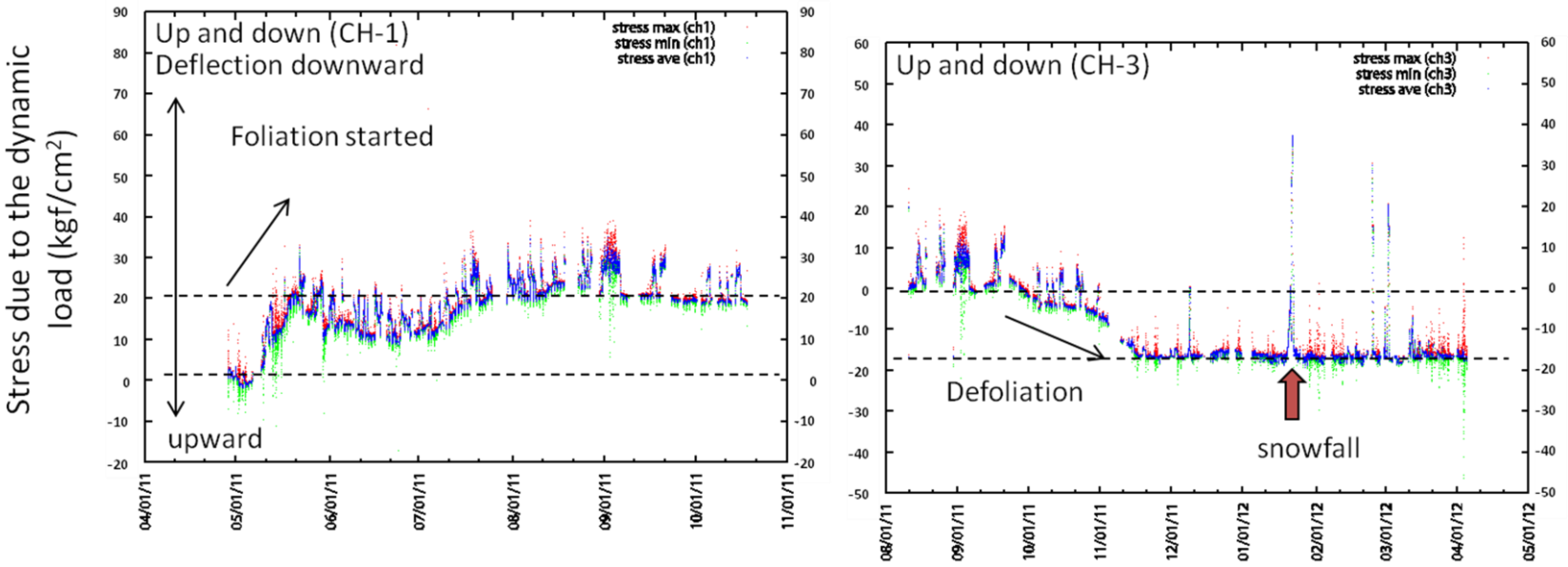

Fig. 21. Changes in the maximum (red), minimum (green), and average stress (blue) values of each file plotted against time for branches of *F. crenata*. For CH-1 and 3, the average value increased by 20 kg/cm^2 in May (foliation) and decreased in autumn (defoliation). Snowfall resulted in an increase of 50 kg/cm^2. The upper and lower broken lines represent the basal values of a branch with and without leaves, respectively. At the upper broken lines, the stress due to the branch's own weight already acts on the branch. The limit of stress the branch can bear is about 472.7 kg/cm^2 above the value of these lines.

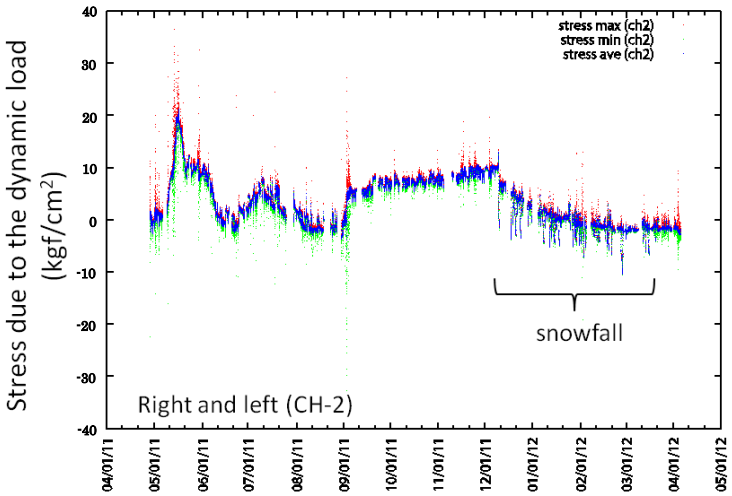

Fig. 22. The changes of the maximum, minimum, and average stress values of each file plotted against time for a branch of *F. crenata*. For CH-2, the average value returned to the initial value after a period of increase.

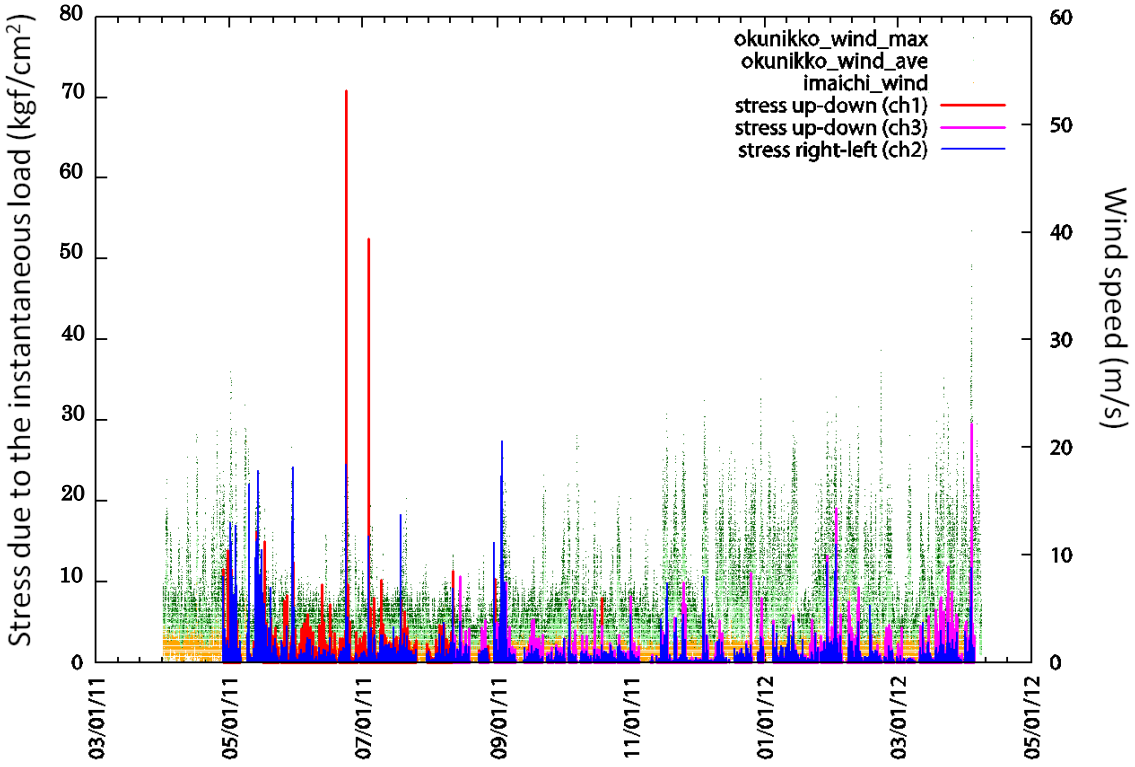

Fig. 23. The difference between the maximum and average values of each data file (lines) and the wind speed data in Nikko (dots). The red and pink lines represent the stresses in the up–down direction and the blue lines represent the stresses in the right–left direction. These data show how much the branch was deflected due to momentary loads (e.g., wind, rain, falling objects). The maximum of the value due to dynamic loads was 71 kgf/cm^2.

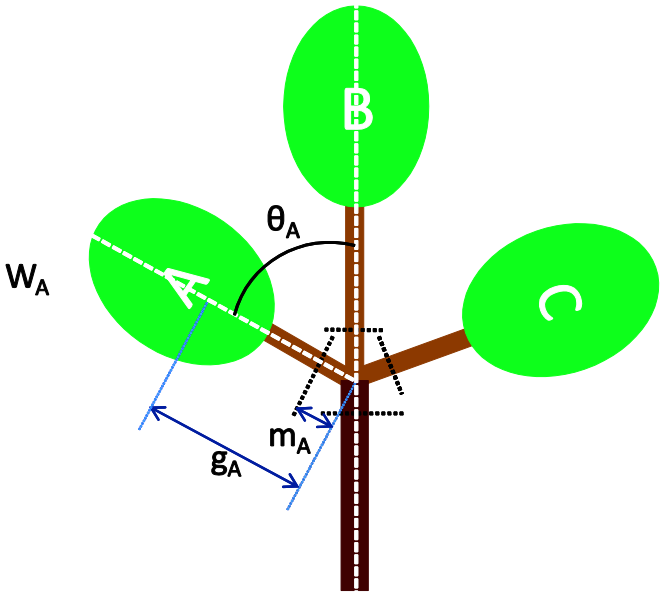

Fig. 24. Overhead view of the proposed branching system scheme. A mother branch has several daughter branches, here labelled as A, B, and C. The branch's spatial arrangement is within a horizontal plane. The weight of daughter branches is defined as W_A, W_B, and W_C and the distances between the center of gravity and the base of each daughter are g_A, g_B, and g_C. The branching angles of each daughter are θ_A, θ_B, and θ_C and the distances between the branching point and the measurement points are m_A, m_B, m_C, and m_M.

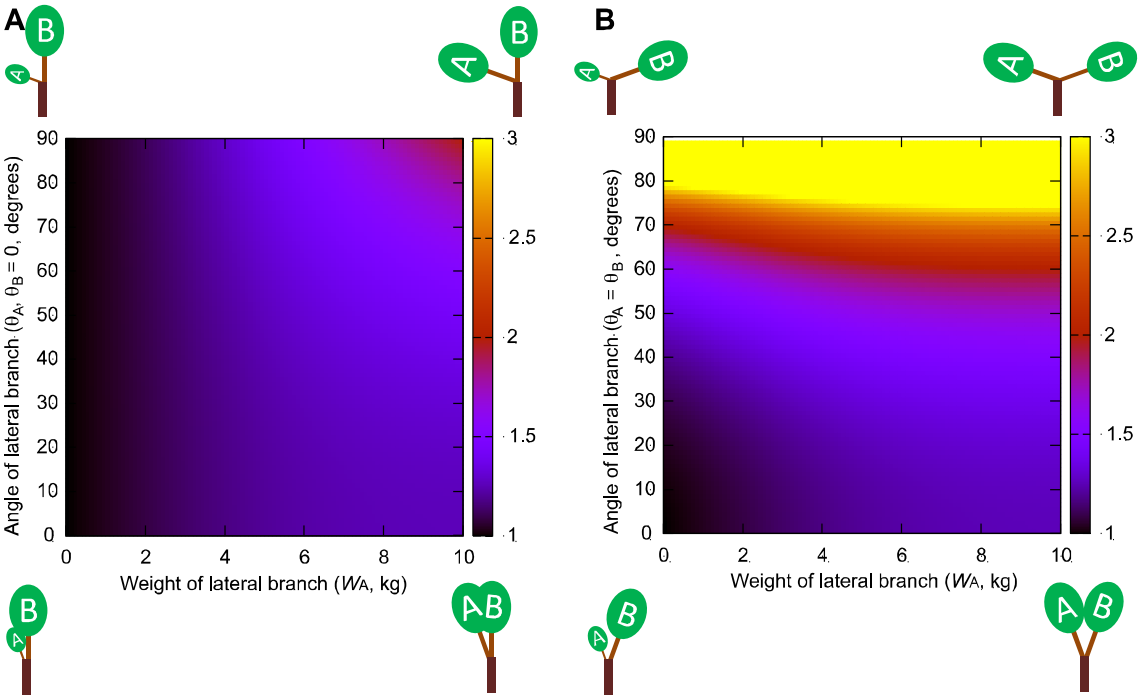

Fig. 25. Daughter/mother ratios based on assumptions of the uniform stress model for two daughters. Daughter/mother ratios based on assumptions of the uniform stress model plotted in palette maps. The range of values for daughter/mother ratios is represented by a range of colors. Values greater than 3 are shown in yellow. This plot shows two daughters (A and B) with weights denoted by W_A and W_B. The weight of daughter B is fixed at 10 kg, and the weight of daughter A is set to vary from 0 to 10 kg. m_M and m_i are 1 cm. (A) θ_B was fixed at zero, θ_A was set to vary from 0.1 to 90°. (B) The angles of daughter A and B are set as $\theta_A = \theta_B$ and to vary from 0.1 to 90°.

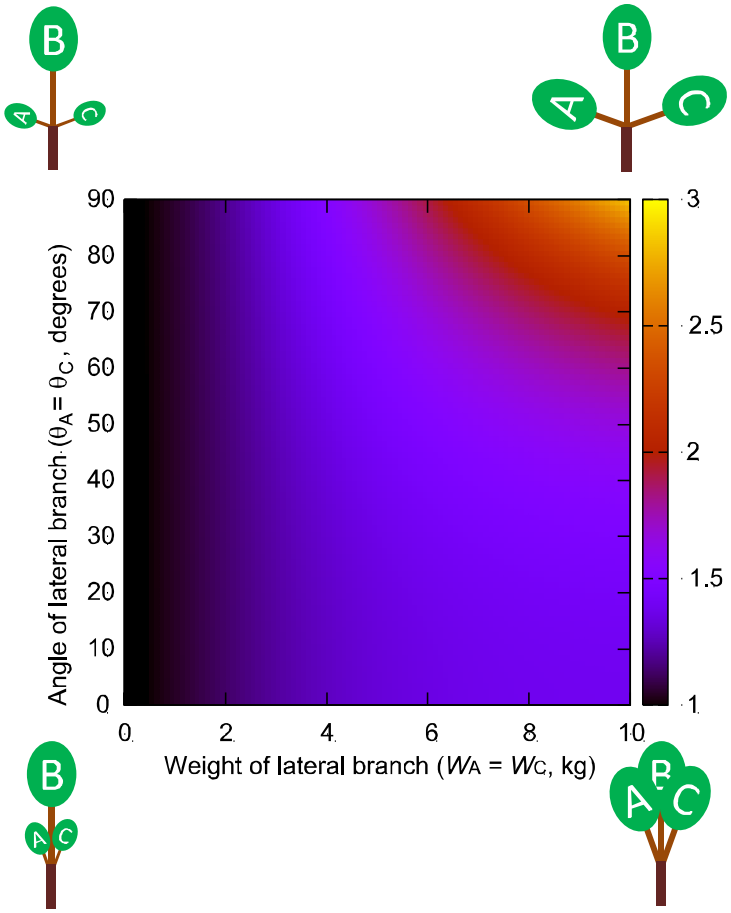

Fig. 26. Daughter/mother ratios based on assumptions of the uniform stress model for three daughters. Daughter/mother ratios based on assumptions of the uniform stress model for three daughters: A, B, and C. Different values of the daughter/mother ratio are represented by different colors. Values greater than 3 are shown in yellow. The angles of daughters A and C are set as $\theta_A = \theta_C$ and to vary from 0.1 to 90°.The weight of daughter B is fixed at 10 kg, and the weights of daughters A and C are set as $W_A = W_C$ and to vary from 0 to 10 kg. m_M and m_i are 1 cm.

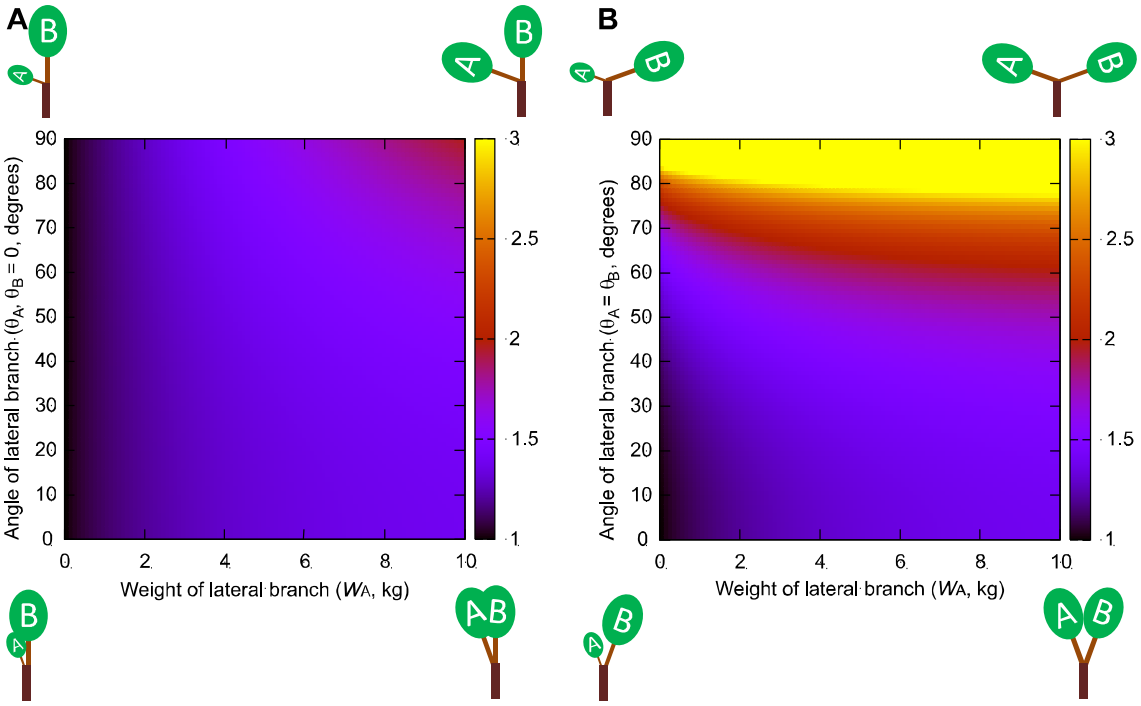

Fig. 27. Daughter/mother ratios based on assumptions of the elastic similarity model for two daughters. Daughter/mother ratios based on the assumptions of the elastic similarity model for two daughters, A and B, with weights W_A and W_B. Different values of the daughter/mother ratio are represented by different colors. Values greater than 3 are shown in yellow. The weight of daughter B is fixed at 10 kg and the weight of daughter A is set to vary from 0 to 10 kg. (A) θ_B was fixed at zero, θ_A was set to vary from 0.1 to 90°. (B) The angles of daughter A and B are set as $\theta_A = \theta_B$ and to vary from 0.1 to 90°.

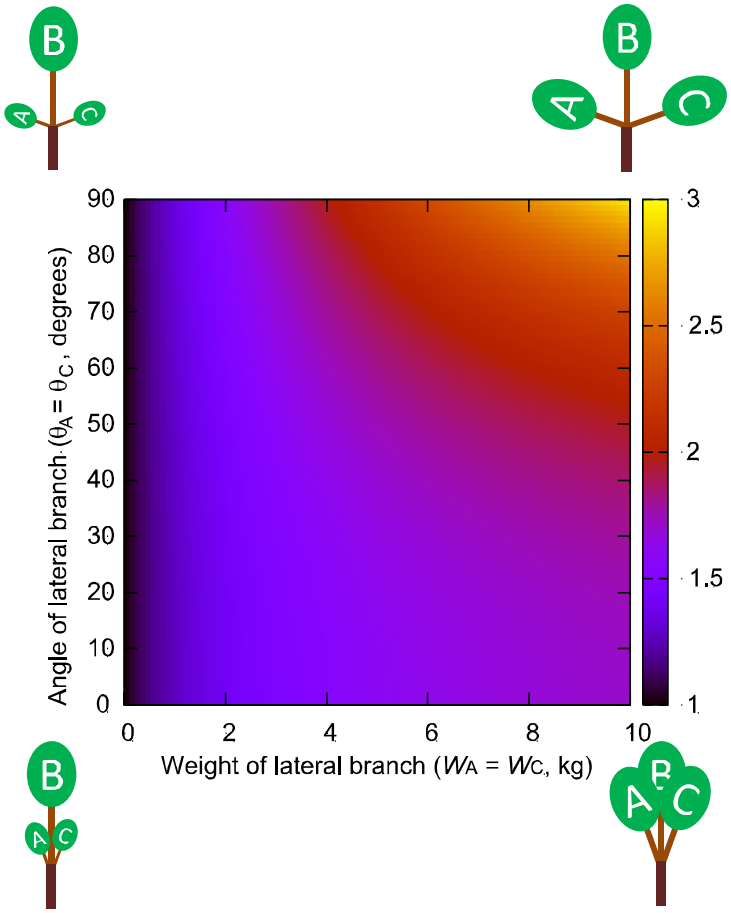

Fig. 28. Daughter/mother ratios based on assumptions of the elastic similarity model for three daughters. Daughter/mother ratios based on assumptions of the elastic similarity model for three daughters, A, B, and C. Different values of the daughter/mother ratio are represented by different colors. Values greater than 3 are shown in yellow. The angles of daughters A and C are set as $\theta_A = \theta_C$ and to vary from 0.1 to 90°. The weight of daughter B is fixed at 10 kg, and the weights of daughters A and C are set as $W_A = W_C$ and to vary from 0 to 10 kg. m_M and m_i are 1 cm.

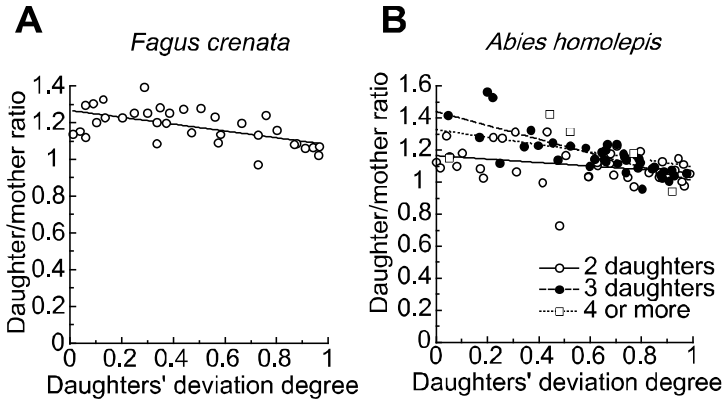

Fig. 29. Daughter/mother ratios vs. daughters' degrees of deviation. Daughter/mother ratios vs. daughters' degree of deviation in (A) *F. crenata* and (B) *A. homolepis*. The number of daughters branching from a mother branch is two in *F. crenata*, and two (open circles), three (filled circles), and four to five (open squares) in *A. homolepis*.

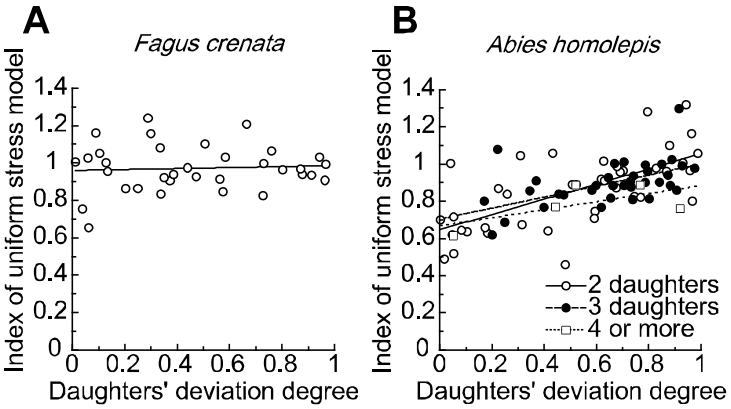

Fig. 30. Indices of the uniform stress model vs. daughters' degrees of deviation. Indices of the uniform stress model vs. daughters' degrees of deviation in (A) *F. crenata* and (B) *A. homolepis*. The theoretical value of the index is 1.0, independent of daughters' degrees of deviation.

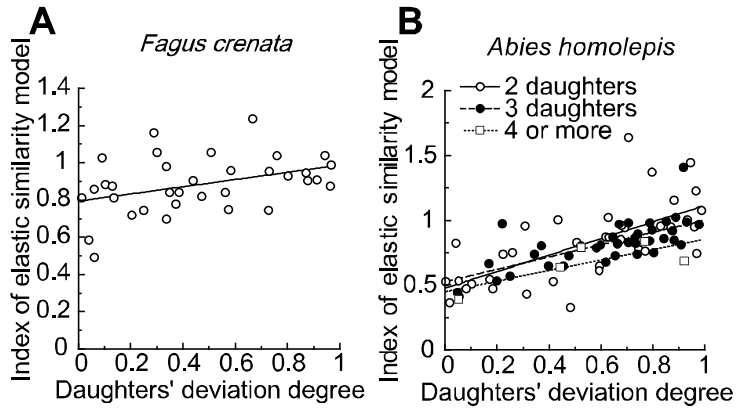

Fig. 31. Elastic similarity model indices relative to daughters' degrees of deviation. Elastic similarity model indices plotted against daughters' degrees of deviation in (A) *F. crenata* and (B) *A. homolepis*. The theoretical value of the index is 1.0 independent of daughters' degrees of deviation.

8. Appendix

Elimination of the effect of shear stress from the measured Young's modulus

The σ/δ data were modified to eliminate the effect of shear stress from the calculated value of Young's modulus (Timoshenko 1955).

When a beam (or branch) with simply supported ends is loaded at the center of the two supported ends, the deformation due to the bending moment (δ_M) is formulated as

$$\delta_M = \frac{P_b l_s^3}{48EI}, \tag{A1}$$

where I is the moment of inertia of area. Deformation due to the shear stress (δ_S) is formulated as

$$\delta_S = \frac{P_b l_s}{3GA}, \tag{A2}$$

where G is the shear modulus and A is the cross-sectional area of the beam.

The total deflection δ is the sum of the two deformations above and can be described as

$$\delta = \frac{P_b l_s^3}{48EI}\left(1 + \frac{E\pi d^4}{4GAl_s^2}\right) = \frac{P_b l_s^3}{48EI}\left(1 + \frac{E}{G}\cdot\left(\frac{d}{l_s}\right)^2\right). \tag{A3}$$

The latter member in the bracket on the right side is the element of the shear stress. The relationship between the load and the deflection obtained from the bending test is the total deflection δ. Here, the E/G of the greenwood of angiosperm seems to be roughly 10–20. Therefore, δ_M can be calculated from the δ using the following equation:

$$\delta_M = \delta \cdot \frac{1}{\left(1 + \frac{E}{G}\cdot\left(\frac{d}{l_s}\right)^2\right)} \tag{A4}$$

Then substituting δ_M of equation (A4) for δ of (13), the actual modulus of elasticity for bending can be calculated as

$$E = \frac{4P_{\mathrm{b}} {l_{\mathrm{s}}}^3}{3\pi d^4 \delta} \cdot \left(1 + \frac{E}{G} \cdot \left(\frac{d}{l_{\mathrm{s}}} \right)^2 \right). \quad \text{(A5)}$$

For *E*/*G*, the data were not obtained for the greenwood of *F. crenata* in the literature. Instead, the data for dry wood were taken from Sawada (1958), which provided values of 24 (Sawada 1958) or 15.7 (Yamai 1959) for (E_L/G_{LT}), and 13 (Sawada 1958) or 11.9 (Yamai 1959) for E_L/G_{LR}. For a different deciduous species, *Fraxinus lanuginosa*, the *E/G* of greenwood was slightly higher than that of air-dried wood. Specifically, the *E/G* of greenwood was 7.3–12.8–23.0 (min–ave–max) and that of air-dried wood was 7.6–12.0–15.9 (min–ave–max). Therefore, the *E/G* of the greenwood of *F. crenata* should be higher than that of air-dried wood and could be roughly within the range of 15–30. Therefore, I set the *E/G* of the greenwood of *F. crenata* to 20 or 30 for the modification of Young's modulus using equation (A5). Literature values of the *E/G* of the greenwood of *A. homolepis* were not found. Therefore, I also used the value 20 or 30 for the *E/G* of greenwood as the value that added a little value to 16.7 which is the general E_L/G_{LR} value for the dry wood of gymnosperm (Sawada 1983). These values cannot be confirmed to be accurate, but they may not differ greatly from the real values.

9. Acknowledgements

I would like to express my deepest gratitude to Dr. Masaki Tateno for all his guidance and support for my study; without him, I would not have been able to complete my studies. Special thanks also go to Dr. Futoshi Ishiguri of Utsunomiya University for valuable advices on mechanical testing. I am grateful to Dr. Tomokazu Tani of Joetsu University of Education, who once belonged to the Nikko botanical garden, for technical instruction and kind encouragement on my work. I deeply appreciate Mr. Takeshi Ono and Mr. Hidetoshi Samata, who gave me technical advice on strain gauge measurements. I also thank former and current members of the Nikko Botanical Garden for their useful discussions and support during fieldwork. I also express my gratitude to the Sasakawa Scientific Research Grant and Yamaguchi Educational and Scholarship Foundation for financially supporting my Ph. D. study.

I would like to express my gratitude to my family for their moral support and kind encouragement.

10. Literature cited

Anten, N., & Schieving, F. (2010). The role of wood mass density and mechanical constraints in the economy of tree architecture. *The American Naturalist, 175*(2), 250-260.

Bertram, J. (1989). Size-dependent differential scaling in branches: The mechanical design of trees revisited. *Trees-Structure and Function, 3*(4), 241-253.

Blackburn, G. R. A. (1997). The growth and mechanical response of trees to wind loading. Ph.D. dissertation, Manchester University, UK.

Bonser, R., & Ennos, A. (1998). Measurement of prestrain in trees: Implications for the determination of safety factors. *Functional Ecology, 12*(6), 971-974.

Brüchert, F., Becker, G., & Speck, T. (2000). The mechanics of Norway spruce [*Picea abies* (L.) Karst]: mechanical properties of standing trees from different thinning regimes. *Forest Ecology and Management*, 135, 45-62.

Brüchert, F., & Gardiner, B. (2006). The effect of wind exposure on the tree aerial architecture and biomechanics of sitka spruce (*Picea sitchensis*, Pinaceae). *American Journal of Botany*, *93*(10), 1512-1521.

Burgert, I., & Fratzl, P. (2009). Plants control the properties and actuation of their organs through the orientation of cellulose fibrils in their cell walls. *Integrative and Comparative Biology, 49*, 69-79.

Dahle, G. A., & Grabosky, JC. (2010). Allometric patterns in *Acer platanoides* (Aceraceae) branches. *Trees-Structure and Function,* doi: 10.1007/s00468-009-0401-5.

Dean, T. J., & Long, J. N. (1986). Validity of constant-stress and elastic-instability principles of stem formation in pinus-contorta and trifolium-pratense. *Annals of Botany, 58*(6), 833-840.

Dean, T., Roberts, S., Gilmore, D., Maguire, D., Long, J., O'Hara, K., et al. (2002). An

evaluation of the uniform stress hypothesis based on stem geometry in selected north american conifers. *Trees-Structure and Function, 16*(8), 559-568.

Ennos, A. (1997). Wind as an ecological factor. *Trends in Ecology & Evolution 12*(3), 108-111.

Evans, J., Senft, J., & Green, D. (2000). Juvenile wood effect in red alder: Analysis of physical and mechanical data to delineate juvenile and mature wood zones. *Forest Products Journal, 50*(7-8), 75-87.

Evans, L. S., Kahn-Jetter, Z., Torres, J., Martinez, M., & TARSIA, P. (2008). Mechanical stresses of primary branches: A survey of 40 woody tree and shrub species. *Trees-Structure and Function, 22*, 283-289.

Färber, J., Lichtenegger, H., Reiterer, A., Stanzl-Tschegg, S., & FRATZL, P. (2001). Cellulose microfibril angles in a spruce branch and mechanical implications. *Journal of Materials Science, 36*, 5087-5092.

Gartner, B. L. (1995). Patterns of xylem variation within a tree and their hydraulic and mechanical consequences. *In* B. L. Gartner [ed.], Physiological Ecology Series; Plant stems: Physiology and functional morphology, 125-149. Academic Press, San Diego, California, USA.

Givnish, T. (1988). Adaptation to sun and shade - a whole-plant perspective. *Australian Journal of Plant Physiology, 15*(1-2), 63-92.

Greenhill, G. (1881) Determination of the greatest height consistent with stability that a vertical pole or mast can be made, and of the greatest height to which a tree of given proportions can grow. *Proceedings of the Cambridge Philosophical Society, 4*, 65-73

Hale, S. E., Gardiner, B. A., Wellpott, A., Nicoll, B. C., & Achim, A. (2012). Wind loading of trees: Influence of tree size and competition. *European Journal of Forest Research 131*(1): 203-217.

Horn, H. (2000). Twigs, trees, and the dynamics of carbon in the landscape. *Scaling in*

Biology (pp. 199-220)

Huang, Y., Chen, S., Kuo-Huang, L., & Lee, C. (2005). Growth strain in the trunk and branches of chamaecyparis formosensis and its influence on tree form. *Tree Physiology, 25*(9), 1119-1126.

Jacobs, M. R. (1954). The effect of wind sway on the form and development of *Pinus radiata* D. Don. *Australian Journal of Botany*, 2, 35–51.

James, K. R., & Kane, B. (2008). Precision digital instruments to measure dynamic wind loads on trees during storms. *Agricultural and Forest Meteorolog*y, *148*(6-7), 1055-1061.

King, D., & Loucks, L. (1978). Theory of tree bole and branch form. *Radiation and Environmental Biophysics,15*(2), 141-165.

King, D. (1981). Tree dimensions - maximizing the rate of height growth in dense stands. *Oecologia, 51*(3), 351-356.

King, D. (1986). Tree form, height growth, and susceptibility to wind damage in acer-saccharum. *Ecology*, *67*, 980-990.

Koizumi, A, & Ueda, K. (1987). Bending and Torsional Properties of Logs. *Research Bulletins of the College Experiment Forests Hokkaido University, 44*(1), 355-380

Kozak, A., & Smith, J. (1993). Standards for Evaluating Taper Estimating Systems. *Forestry Chronicle, 69*, 438-444

Lundqvist, L., & Valinger, E. (1996). Stem Diameter Growth of Scots Pine Trees after Increased Mechanical Load in the Crown during Dormancy and (or) Growth. *Annals of Botany*, 77, 59-62.

Mattheck, C., Bethge, K., & Scafer, J. (1993). Safety factors in trees. *Journal of Theoretical Biology*, *165*, 185-189

McMahon, T. (1973). Size and shape in biology. *Science (New York, N.Y.), 179*(4079), 1201-1204.

McMahon, T. (1975). Allometry and biomechanics - limb bones in adult ungulates. *American Naturalist, 109*(969), 547-563.

McMahon, T., & Kronauer, R. (1976). Tree structures - deducing principle of mechanical design. *Journal of Theoretical Biology, 59*(2), 443-466.

Meng, S. X., Lieffers, V. J., Reid, D. E. B., Rudnicki, M., Silins, U., & Jin, M. (2006). Reducing stem bending increases the height growth of tall pines. *Journal of Experimental Botany, 57*(12), 3175-3182.

Metzger, K. (1893) Der Wind als massgebender Faktor für das Wachstum der Bäume. *Mündener Forstliche, 3*, 35–86

Moore, J., Gardiner, B., Blackburn, G., Brickman, A., & Maguire, D. (2005). An inexpensive instrument to measure the dynamic response of standing trees to wind loading RID H-3629-2011. *Agricultural and Forest Meteorology*, *132*(1-2), 78-83.

Nikinmaa, E. (1992). Analyses of the growth of scots pine: Matching structure with function. *Acta Forestalia Fennica,235*, 1-68.

Niklas, K. (1994)a. The allometry of safety-factors for plant height. *American Journal of Botany, 81*(3), 345-351.

Niklas, K. (1994)b. Interspecific allometries of critical buckling height and actual plant height. *American Journal of Botany, 81*(10), 1275-1279. doi:10.2307/2445403

Niklas, K. (1995). Size-Dependent Allometry of Tree Height, Diameter and Trunk-Taper. *Annals of Botany, 3*, 217-227.

Niklas, K. (1997)a. Mechanical properties of black locust (*Robinia pseudoacacia* L.) wood. size- and age-dependent variations in sap- and heartwood. *Annals of Botany*, *79*(3), 265-272.

Niklas, K. (1997)b. Size- and age-dependent variation in the properties of sap- and heartwood in black locust (*Robinia pseudoacacia* L.). *Annals of Botany*, *79*(5), 473-478.

Niklas, K. J. (1999). Changes in the factor of safety within the superstructure of a dicot tree. *American Journal of Botany, 86*(5), 688.

Niklas, K. (2000). Computing factors of safety against wind-induced tree stem damage. *Journal of Experimental Botany*, *51*, 797-806

Niklas, K. J. (2000). Wood biomechanics and anatomy of pachycereus pringlei. *American Journal of Botany, 87*(4), 469-481.

Niklas, K., & Spatz, H. (2000). Wind-induced stresses in cherry trees: Evidence against the hypothesis of constant stress levels. *Trees-Structure and Function, 14*(4), 230-237.

Niklas, K., & Spatz, H. (2004). Growth and hydraulic (not mechanical) constraints govern the scaling of tree height and mass. *Proceedings of the National Academy of Sciences of the United States of America*, *101*(44), 15661-15663.

Plomion, C., Leprovost, G., & Stokes, A. (2001). Wood formation in trees. *Plant Physiology*, *127*, 1513-1523.

Putz, F., Coley, P., Lu, K., Montalvo, A., & Aiello, A. (1983). Uprooting and snapping of trees - structural determinants and ecological consequences. *Canadian Journal of Forest Research-Revue Canadienne De Recherche Forestiere*, *13*(5), 1011-1020.

Reiterer A., Lichtenegger, H., Tschegg, S., & Fratzl, P. (1999). Experimental evidence for a mechanical function of the cellulose microfibril angle in wood cell walls. *Philosophical Magazine A-Physics of Condensed Matter Structure Defects and Mechanical Properties*, *79*, 2173-2184.

Richter, J. (1970). The notebooks of Leonardo da Vinci. Dover, New York

Ryan, M. & Yoder, B. (1997). Hydraulic limits to tree height and tree growth. *Bioscience*. doi: 10.2307/1313077

Ryan, M., Phillips, N., & Bond, B. (2006). The hydraulic limitation hypothesis revisited. *Plant*

Cell and Environment, *29*(3), 367-381.

Sawada, M. (1958). Study on mechanical properties of the wood. *Ringyoushikenjoukenkyuuhoukoku* (*Bulletin of the Forestry and Forest Products Research Institute*), *108*,115-224.

Sawada, M. (1983). Deformation behavior of wood. *Zairyou*, *32*, 838-847.

Schaetzl, R., Johnson, D., Burns, S., & Small, T. (1989). Tree uprooting - review of terminology, process, and environmental implications. *Canadian Journal of Forest Research-Revue Canadienne De Recherche Forestiere*, *19*(1), 1-11.

Sone, K., Noguchi, K., & Terashima, I. (2005). Dependency of branch diameter growth in young acer trees on light availability and shoot elongation. *Tree Physiology*, *25*(1), 39-48.

Sone, K., Suzuki, A. A., Miyazawa, S., Noguchi, K., & Terashima, I. (2009). Maintenance mechanisms of the pipe model relationship and leonardo da vinci's rule in the branching architecture of acer rufinerve trees. *Journal of Plant Research*, *122*(1), 41-52.

Taneda, H., & Tateno, M. (2004). The criteria for biomass partitioning of the current shoot: water transport versus mechanical support. *American Journal of Botany*, *91*(12), 1949-1959.

Tateno, M. (1991). Increase in lodging safety factor of thigmomorphogenically dwarfed shoots of mulberry tree. *Physiologia Plantarum*, *81*(2), 239-243.

Tateno, M., & Bae, K. (1990). Comparison of lodging safety factor of untreated and succinic acid 2,2-dimethylhydrazide-treated shoots of mulberry tree. *Plant Physiology (Bethesda)*, *92*(1), 12-16.

Timoshenko, S. (1955) Strength of Materials Part 1: Elementary Theory and Problems, 3rd ed. Van Nostrand Reinhold Inc., New York, USA.

Valinger, E., Lundqvist, L., & Sundberg, B. (1994). Mechanical stress during dormancy stimulates stem growth of Scots pine seedlings. *Forest Ecology and Management*, 67, 299-303.

Valinger, E., & Pettersson, N. (1996). Wind and snow damage in a thinning and fertilization experiment in *Picea abies* in southern Sweden. *Forestry*, 69(1), 25-33.

van Gelder, H., Poorter, L., & Sterck, F. (2006). Wood mechanics, allometry, and life-history variation in a tropical rain forest tree community. *The New Phytologist, 171*(2), 367-378.

Watt, M. S., Kirschbaum, M. U. F. (2011). Moving beyond simple linear allometric relationships between tree height and diameter. *Ecological Modelling*. doi: 10.1016/j.ecolmodel.2011.10.011

West, G. B., & Brown, J. H. (2005). The origin of allometric scaling laws in biology from genomes to ecosystems: towards a quantitative unifying theory of biological structure and organization. *Journal of Experimental Biology*, *208*, 1575-1592

Wilson, B. F., & Archer, R. R. (1977). Reaction wood: Induction and mechanical action. *Annual Review of Plant Physiology, 28*(1), 23-43. doi:10.1146/annurev.pp.28.060177.000323

Yamai, R. (1959). Study on compression anisotropy of the wood. *Ringyoushikenjoukenkyuuhoukoku* (*Bulletin of the Forestry and Forest Products Research Institute*), *113*, 58-110.

Yamamoto, H., Okuyama, T., & Iguchi, M. (1989). Measurement of growth stresses on the surface of a leaning stem. *Mokuzai Gakkaishi*, *35*, 595-601.

Yamamoto, M., Miyano, H., Maeda, N. & Moriizumi, S. (1992). Bending test of larch log and two-faced sawn lumber in full size (1). *Journal of Hokkaido Forrest Products Research Institute, 6*(3): 17-21. Website http://www.fpri.hro.or.jp/rsjoho/26960012001.pdf

Yoneda, M. (1987). Strength tests on poles and two-surface sawn lumbers from smaller diameter softwood logs. *Journal of Hokkaido Forest Products Research Institute*, *1*(4), 1-11. Website http://www.fpri.hro.or.jp/rsjoho/22122009001.pdf

Yoshida, M., & Okuyama, T. (2002). Techniques for measuring growth stress on the xylem surface using strain and dial gauges. *Holzforschung, 56*(5), 461-467.

Yoshino, A., Shibata, N., & Toda, K. (2010). Development of the use technology to civil engineering structure or tree bridge, mainly involving thinned wood of Japanese larch. *Research Report of Nagano Prefecture Forestry Research Center*, *24*. Website http://www.pref.nagano.lg.jp/ringyosogo/seika/kenkyu/mokuzai/documents/moku-24-3.pdf